catalysts

MDPI

Review

Catalytic Hydrogenation of CO_2 to Methanol: A Review

Menghao Ren, Yanmin Zhang, Xuan Wang * and Hengshan Qiu *

Engineering Research Center of Advanced Functional Material Manufacturing of Ministry of Education, School of Chemical Engineering, Zhengzhou University, Zhengzhou 450001, China; 18438623187@163.com (M.R.); zhangfan125@foxmail.com (Y.Z.)

* Correspondence: wangxuan@zzu.edu.cn (X.W.); hsqiu@zzu.edu.cn (H.Q.); Tel.: +86-371-6778-1801 (H.Q.)

Abstract: High-efficiency utilization of CO_2 facilitates the reduction of CO_2 concentration in the global atmosphere and hence the alleviation of the greenhouse effect. The catalytic hydrogenation of CO_2 to produce value-added chemicals exhibits attractive prospects by potentially building energy recycling loops. Particularly, methanol is one of the practically important objective products, and the catalytic hydrogenation of CO_2 to synthesize methanol has been extensively studied. In this review, we focus on some basic concepts on CO_2 activation, the recent research advances in the catalytic hydrogenation of CO_2 to methanol, the development of high-performance catalysts, and microscopic insight into the reaction mechanisms. Finally, some thinking on the present research and possible future trend is presented.

Keywords: carbon dioxide; hydrogenation; heterogeneous catalysis; methanol synthesis; catalysts; reaction mechanism

Citation: Ren, M.; Zhang, Y.; Wang, X.; Qiu, H. Catalytic Hydrogenation of CO_2 to Methanol: A Review. *Catalysts* **2022**, *12*, 403. https://doi.org/10.3390/catal12040403

Academic Editor: Maria A. Goula

Received: 18 March 2022
Accepted: 4 April 2022
Published: 6 April 2022

Publisher's Note: MDPI stays neutral with regard to jurisdictional claims in published maps and institutional affiliations.

Copyright: © 2022 by the authors. Licensee MDPI, Basel, Switzerland. This article is an open access article distributed under the terms and conditions of the Creative Commons Attribution (CC BY) license (https://creativecommons.org/licenses/by/4.0/).

1. Introduction

1.1. Background

CO_2 can be used as condensing agent (dry ice), protective gas for fruit preservation, fizzy gas in carbonated drinks, solvent for homogeneous catalysis (in a supercritical state), and reactant for the mineralization and carbonate-based chemicals [1,2]. In recent decades, booming research interests in CO_2 were stimulated by its greenhouse effect on global climate change [3]. The global atmospheric CO_2 has been speedily rising since the 1950s and has doubled nowadays (212 ppm in 1958 vs. 445 ppm in 2021) [4]. Another doubling was predicted, according to the model of the high emission scenario, to be reached by the year 2100 [5]. The greenhouse effect of atmospheric gases is originated from their absorption of infrared (IR) irradiation from the earth's surface. Any IR-active molecule such as H_2O, CH_4, CO_2, and NO_x can be a candidate for greenhouse gases with the ability to absorb photons depending on the dynamic transition dipole and the freedom of vibrations [5]. An exception is H_2O, of which the natural greenhouse effect has made the earth's temperature appropriate for its biosystem, and equilibrium has been reached because of the huge surface of oceans [5]. Among other greenhouse gases, CO_2 plays the dominant role because of its overwhelming emission related to modern human life [6]. Control of CO_2 emission is urgent to alleviate the greenhouse effect. In recent years, carbon capture and storage (CCS) technologies have been developed to separate CO_2 from either chemical processes or combustion products, followed by recycling or storage [2]. Recently, CO_2 capture directly from the air also caught some scientific and practical interest [7,8]. However, though effectively reducing the emission of CO_2 to some extent, CCS does not provide the final solution because of the high cost and potential risk of leakage. Conversion of the captured CO_2 to value-added chemicals, in this situation, draws the CO_2 back to carbon recycling, providing a sustainable solution [9].

As the highest oxidation state of carbon element, CO_2 shows significant thermodynamic stability with the formation enthalpy of 396 kJ/mol [10]. Therefore, converting CO_2 to thermodynamically more stable chemicals such as Na_2CO_3, $NaHCO_3$, NH_4HCO_3, and salicylic acid provides a relatively feasible way for manufacturers to deal with massive CO_2 emissions [11–13]. An alternative way is to convert CO_2 to energetically undesired but value-added chemicals such as methanol [14–16], methane [17–19], and hydrocarbons [20–24], in processes in which excess energy must be injected into the CO_2 molecules. The candidates possessing energy are generally fossil fuels (petroleum, coal, and natural gas) or renewable resources (solar energy, wind energy, hydropower, geothermal power, biomass energy, etc.). For instance, the following reaction:

$$CO_2(g) + 2H_2(g) \rightarrow CH_3OH(g) + H_2O(g) \quad \Delta H = -49.3 \text{ kJ/mol}$$

is thermodynamically favorable. Therefore, technically, the activation (hydrogenation) of CO_2 suffered more likely from kinetics instead of thermodynamics. Similarly, the value of the extremely high bond energy (about 750 kJ/mol for each C=O bond) makes little sense unless a thorough decomposition in the gas phase is considered. The limited use of CO_2 in the chemical industry, however, is mainly due to the consideration of economic factors, such as the investment of equipment, the cost of H_2 production, the low yields of methanol, and accompanied CO_2 emission. Particularly, when renewable H_2 can be produced on a large scale, the hydrogenation of CO_2 will attract more attention from the industry [25].

1.2. Bonding Properties and Activation of CO_2

A neutral CO_2 molecule exhibits a linear geometry with a carbon–oxygen bond length of 1.17 Å [26]. Figure 1 shows the Walsh diagram of CO_2 orbitals, which gives the correlation between the OCO angle and orbital energies [1]. The highest occupied molecular orbital (HOMO) is composed of $1\pi_g$ contributed exclusively from oxygen 2p orbitals. The lowest unoccupied molecular orbital (LUMO) is a hybrid $2\pi_u$. As an electron is transferred to the LUMO of CO_2, the molecule tends to bend according to the change in energy of each orbital. For instance, the CO_2^- anion shows an equilibrium OCO angle of 135° and can be stabilized kinetically (with the activation barrier of 0.4 eV), although its energy is 0.5 eV higher than that of a neutral CO_2 molecule [27,28].

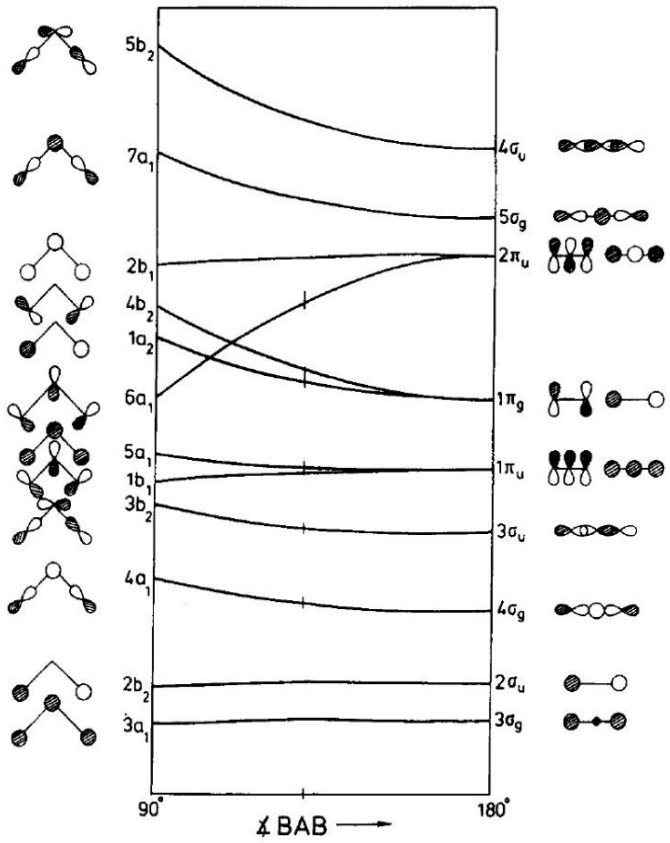


Figure 1. Walsh diagram of CO_2 orbital energies in linear and bent geometries. Reprinted with permission from [1]. Copyright 1996 Elsevier.

CO_2 molecules can be activated on either metal or oxide surfaces. On the metal surface, electrons in the metal are transferred to physisorbed CO_2 resulting in a chemisorbed anionic $CO_2^{\delta-}$ which was thought to be the precursor for CO_2 dissociation and carbonate formation [29]. This process, however, is often accompanied by high activation barrier with the value depending on the metal's work function [1,30]. Steps [31,32], alkali metal promotions (e.g., K, Na) [33,34], coadsorption (e.g., H, O) [35,36] may facilitate the electron transfer. On oxide surfaces, CO_2 adsorption becomes more complicated due to the amphoteric nature of CO_2 and the structural and electronic complexity of oxide surfaces. In general, the carbon atom of the CO_2 molecule, which is more electropositive, tends to bond to the Lewis basic sites (usually the oxygen sites), and the oxygen atoms of the CO_2 molecule to the Lewis acidic sites (usually the cationic sites) [37,38]. As a result, a common adsorbed surface species, besides a physisorbed CO_2, is carbonate with the geometry of monodentate, bidentate, or even a tridentate, depending on the surface atomic arrangement [39]. For instance, on an oxygen terminated surface, only monodentate carbonate is formed, while bidentate species is usually obtained on mixed-terminated or defective surfaces [40].

The first step of CO_2 activation is typically the adsorption of CO_2 on catalyst surfaces which lowers the total energy of the system. The binding energy of CO_2 to the surface strongly influences the coverage of CO_2 on the catalyst surface, as well as the reaction barrier [41]. Stronger binding of CO_2 on the catalyst's surface promotes the surface coverage, but more energy must be injected to activate the intermediate. Therefore, the activation of CO_2 makes sense only if a whole reaction is considered.

1.3. Conversion Route of CO_2 to Value-Added Chemicals

The possible catalytic conversion routes are shown in Figure 2, and the representative reactions along with the typical catalysts are summarized in Table 1. The ultimate products are distributed from methane and formic acid to hydrocarbons (light olefins, liquefied petroleum gas (LPG), gasoline, aromatics, etc.). The most conspicuous intermediates are CH_3OH and CO, owing to the relatively mature technologies of methanol to hydrocarbons (MTH) (including methanol to olefin (MTO), methanol to aromatics (MTA), methanol to gasoline (MTG), etc.) and Fischer Tropsch synthesis (FTS) adopted in the current chemical industry. Methanol often serves as the starting feedstock for several useful chemicals such as gasoline, dimethyl ether, oxymethylene ethers, or as an additive or fuel in engines and fuel cells [42,43]. Recently, methanol was proposed to be the candidate alternative to oil and gas to generate a "methanol economy" [44]. In this situation, the hydrogenation of CO_2 to produce methanol would be one of the key reactions for building energy recycling loops.

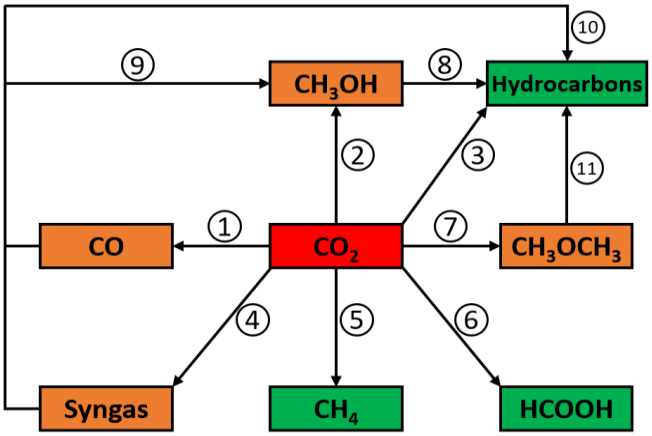


Figure 2. Reaction routes involved in catalytic hydrogenation of CO_2 to value-added chemicals.

Table 1. Detailed reactions shown in Figure 2.

Symbol	Representative Reactions	Reaction Equations	Typical Catalysts and References
①	Reverse Water Gas Shift (RWGS)	$CO_2 + H_2 \rightarrow CO + H_2O$ $\Delta H = 41.5$ kJ/mol	Cu/ZnO/ZrO_2/Ga_2O_3 [45] Carbon FY5 catalyst [46]
②	CO_2-Based Methanol Synthesis	$CO_2 + 3H_2 \rightarrow CH_3OH + H_2O$ $\Delta H = -49.5$ kJ/mol	Cu-based catalysts [14] In_2O_3 based catalysts [16]
③	CO_2-Based Fischer-Tropsch Synthesis (CO_2 FTS)	$CO_2 + 2H_2 \rightarrow (-CH_2-) + H_2O$ $\Delta H = -111$ kJ/mol	Fe-Co catalyst [22], xFeyKzCo(Ru) [21] Mn-Fe-O nanocomposites [47]
④	Dry Reforming of Methane (DRM)	$CO_2 + CH_4 \rightarrow 2CO + 2H_2$ $\Delta H = 247.1$ kJ/mol	Ni/ZSM-5 [48] Ag-La/pCNNT [49]
⑤	CO_2 Methanation	$CO_2 + 4H_2 \rightarrow CH_4 + 2H_2O$ $\Delta H = -165.0$ kJ/mol	Ni/CeO_2 [17,19] Ni-M/Al@Al_2O_3 [18]
⑥	CO_2-Based Formic Acid Synthesis	$CO_2 + H_2 \rightarrow HCOOH$ $H = -31.2$ kJ/mol	Cu/ZnO/Al_2O_3 [50] Pb_2O [51]
⑦	CO_2-Based Dimethyl Ether Synthesis	$CO_2 + 3H_2 \rightarrow CH_3OH + H_2O$ $\Delta H = -49.5$ kJ/mol $2CH_3OH \rightarrow CH_3OCH_3 + H_2O$ $\Delta H = -23.5$ kJ/mol	CuO-Fe_2O_3-CeO_2/HZSM-5 [52] modified Cu/ZnO/Al_2O_3 [53]
⑧	Methanol to Hydrocarbons (MTH)	$2CH_3OH \rightarrow C_2H_4 + 2H_2O$ $\Delta H = -11.72$ kJ/mol $3CH_3OH \rightarrow C_3H_6 + 3H_2O$ $\Delta H = -30.98$ kJ/mol	SAPO-34/HZSM-5 [54] SAPO-34 [55]
⑨	Methanol Synthesis from Syngas	$CO + 2H_2 \rightarrow CH_3OH$ $\Delta H = -90.4$ kJ/mol	Topsøe MK-121 [56] Cu/ZnO/Al_2O_3 [14]
⑩	CO-Based Fischer-Tropsch Synthesis (CO FTS)	$CO + 2H_2 \rightarrow (-CH_2-) + H_2O$ $\Delta H = -152$ kJ/mol	Iron-based catalysts [57] Cobalt-based catalysts [58] Carbon-based catalysts [59]
⑪	Dimethyl ether to Hydrocarbons	$nCH_3OCH_3 \rightarrow 2n[CH_2] + nH_2O$ $\Delta H < 0$	ZSM-5 [60]

2. Recent Advances in Catalyst Research for CO_2 Hydrogenation to Methanol

The main formal difference between the methanol synthesis from CO_2 hydrogenation and CO hydrogenation is the formation of H_2O vapor in the products, as shown in Table 1. The catalysts for catalytic hydrogenation of CO_2 to methanol along with the recently reported reaction promoters are summarized in Table 2. For $Cu/ZnO/Al_2O_3$ catalyst, the presence of water vapor was reported to cause a notable weakening of the stability of the Zn promoter or surface Zn-Cu alloy [61–63]. In addition, despite the fact that the WGS reaction is beneficial to the CH_3OH synthesis from syngas (mainly CO), its reverse reaction converts CO_2 to CO, lowering the yield of methanol [61]. Therefore, a good catalyst for CO_2 hydrogenation to produce methanol must be stable under high water partial pressure and superior against RWGS reaction [64], though water vapor was thought to have a strong influence on the methanol selectivity [65].

Table 2. Summarized catalysts for CO_2 hydrogenation to methanol.

Catalysts	P (MPa)	T (°C)	CO_2:H_2	WHSV ($mL \cdot g^{-1}h^{-1}$)	$Conv_{CO2}$ (%)	$Sel._{CH3OH}$ (%)	STY_{CH3OH} $g \cdot g_{cat}^{-1} \cdot h^{-1}$	Ref.
1 wt% $AuCuO/CeO_2$	3	240	1:3	[a]	6.7	29.6	[a]	[66]
$CuO-ZnO/Al_2O_3$	1	227	1:6	684	13.7	74	[a]	[67]
Cu/CeO_2	3	250	1:3	30,000	1	53	0.045	[68]
60 wt% Cu/AlCeO	3	260	1:3	14,400	~17[b]	~45 [b]	0.381	[43]
$Cu-ZrO_2$	1	230	1:3	50,000	1.6	72.2	~0.017 [b]	[69]
$CuZnZr/CuBr_2$	5	250	1:3	3000	10.7	97.1	~0.1 [b]	[70]
0.5% CuZnZr	4.5	290	1:3	10,800	9.5	76	~0.28 [b]	[71]
co-RhIn/(5In5Al)O	4.5	270	1:3	36,000	7.2	90.8	0.84	[72]
CuZnAlCe	3	250	1:3	12,000	14.2	37.8	0.213	[73]
20% $ZnO-ZrO_2$	2	320	1:3	24,000	6.4	78.5	0.413	[74]
inverse-ZrO_2/Cu	3	220	1:3	48,000	<5	~70	0.524	[75]
3DOM $Cu-ZnO-ZrO_2$	4	180	1:3	18,000	3.5	98	0.217	[65]
$CuO/Ce_{0.4}Zr_{0.6}O_2$	3	220	1:3	10,000	7	96.4	[a]	[76]
In_2O_3	4	200	1:4	9000	0.15	100	~0.004 [b]	[77]
In_2O_3/Co_3O_4	5	285	1:4	15,600	17.3	75	0.65	[78]
In_2O_3/ZrO_2	5	300	1:4	20,000	5.2	99.8	0.295	[79]
$Au^{\delta+}-In_2O_{3-x}$	5	300	1:4	21,000	11.7	67.8	0.47	[80]
$P-In_2O_3$	3	300	1:3	18,000	<3	84.5	0.135	[81]
50 wt% In_2O_3/Co/C-N	2	300	1:3	3000	9.5	88.4	0.0801	[82]
10 wt% Ir/In_2O_3	5	300	1:4	21,000	17.7	70	0.765	[83]
$Au/In_2O_3-ZrO_2$	5	300	1:4	21,000	14.8	70.1	0.59	[84]
Rh/In_2O_3	5	300	1:4	21,000	17.1	56.1	0.5448	[16]
$GaZrO_x$ (27%)	3	330	1:3	24,000	<9	<72.7	<0.61	[85]
$Bi-MnFe_2O_4$	0.1	220	1:3	22,000 [a]	22	61	[a]	[86]
Cu-Zn-Al-K	3	240	1:4	2400 [a]	14	96	0.461	[87]
CuIn-350	3	280	1:3	7500	11.4	80.5	0.197	[88]
Ga_3Ni_5/SiO_2	0.1	200	1:3	[a]	~1.2 [b]	94	~0.075 [b]	[89]
MoS_2	5	180	1:3	~3000 [b]	12.5	94.3	0.13	[90]
$ReOx/TiO_2$	10	200	1:4	4	18	98	7.913	[91]
Pt/H_xMoO_{3-y}	4	200	1:3	[a]	25	33	0.049	[92]
$PdZn/ZnO/SiO_2$	5	260	1:3	60,000	3.3	65.3	0.443	[93]
ZnO_x/ZrO_2	2	300	1:3	9000	~6 [b]	75.1	~0.12 [b]	[94]
$PdZn/ZnO/ZnFe_2O_4$	5	290	1:3	21,600	13.94	55.02	0.593	[95]
MoP/ZrO_2	4	250	1:3	~19,200 [b]	1.4	55.4	~0.05 [b]	[15]

[a] Not available. [b] Estimated based on the data present in the publication.

2.1. Cu-Based Catalysts

Cu-based catalysts, especially $Cu/ZnO/Al_2O_3$ (e.g., typical weight composition of $CuO:ZnO:Al_2O_3$ being 60:22:8 adopted by ICI Ltd.), were originally used as the catalyst for industrial methanol synthesis from syngas (CO, CO_2, and H_2) at ~250 °C and 50–100 bar [96–98]. CO_2 was considered the main carbon source for methanol [99,100], which is possibly a hint that Cu/ZnO catalyst could also be active for methanol synthesis from the hydrogenation of pure CO_2. Nowadays, Cu-based catalysts are still the hotspots in the research field of CO_2 hydrogenation to produce methanol [101] thanks to their all-around unique performance over others. Despite many controversies in understanding the reaction mechanism of commercial $Cu/ZnO/Al_2O_3$ catalysts, progress in catalyst development in recent years has been conspicuous [98,101–106].

The Cu/ZnO catalyst has been thought "a prototype for studying complex promotional interactions in catalysis" [106]. Indeed, both Cu and ZnO have certain activity for methanol synthesis from both CO and CO_2, while only their mixture shows superior performance [97,107]. The consequence of the mixture can be: (1) gas-dependent morphological changes of the active component; (2) support-induced strain; and (3) strong metal–support interaction (SMSI) effect [106]. The consequence includes well-dispersed and stabilized Cu on ZnO, partially oxidized Cu species, creation of oxygen vacancies [108], and formation of ZnO–Cu interface and Zn–Cu alloy [98,106]. Number of strategies were designed revolving around modifying the intrinsic activity of copper in the catalyst, including development of new synthesis methods [109–116], adoption of various support materials [68,115,117,118], and promoters [87,119,120] to enable new structures and morphologies [68,112,121,122], more homogeneous and stable particles size [123,124], tunable metal–oxide interface [125–128], etc.

2.1.1. Preparation Methods

A selective synthesis method was adopted by Tada et al. to prepare an amorphous $Cu_aZr_{1-a}O_b$ catalyst [111]. The method was originally based on an incipient wetness impregnation, followed by drying and calcination (see Figure 3). The main point was emphasized by low calcination temperature and low metal loading. The low calcination temperature enables the formation of interfacial sites between metal and support that were supposed to be the active sites for CO_2-based methanol synthesis. The low metal loading (up to the solubility limit of metal in oxide support) can essentially prevent the formation of crystalline CuO particles and tune the interfacial sites between metal and supports during H_2 reduction.

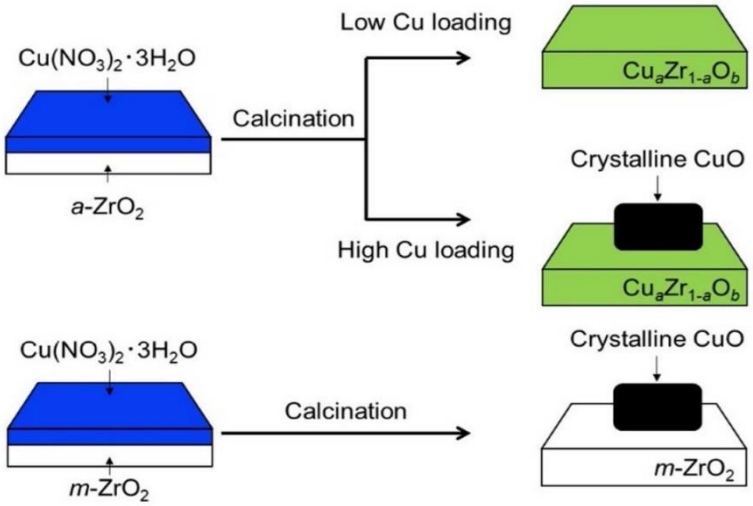


Figure 3. Proposed formation mechanism of $Cu_aZr_{1-a}O_b$, $CuO/Cu_aZr_{1-a}O_b$, and $CuO/m\text{-}ZrO_2$. Reprinted with permission from ref. [111]. Copyright 2018 American Chemical Society.

Yu et al. compared the performance of Cu/SiO_2 catalysts prepared by the ammonia evaporation (AE) method and flame spray pyrolysis (FSP) method [112]. The high temperature in the FSP method facilitates high specific surface area and the formation of mixed oxides and is therefore suited for modulating metal–support interactions [129,130]. Specifically, a distorted Cu-O-Si structure formed in the Cu/SiO_2 stabilizes Cu^+ species, which are closely correlated with the formation of intermediates and methanol. As a result, the FSP sample contains 5 times higher surface Cu^+ species than in the AE sample, leading to a significant enhancement of methanol selectivity. By comparison, Cu-based catalysts prepared through the aerosol-assisted sol–gel (AASG) process possess rich spherical and mesostructured microparticles (see Figure 4 for a schematic view of the AASG process), achieving highly dispersed open mesopores and promoters (e.g., Zn and Ga) [121]. The active component (Cu) was directly introduced by impregnation or incorporated in the precursor solution, which markedly simplifies the synthesis process. The following calcination leads to the enrichment of dispersed Cu species on the catalyst surface. The catalytic activity of resulted catalysts was ascribed to the formation of the sites that are active for methanol synthesis and inactive for reverse water gas shift reaction. The formation of the active sites was originally promoted by the structure promoter (e.g., Zn and Ga) and by the preparation method as well. Likewise, the precursor phase has a strong influence on the activity of the final catalyst. A Zincian georgeite precursor was adopted to synthesize Cu/ZnO catalysts and yielded a high content of exposed Cu sites and intimated Cu–ZnO interface [110].

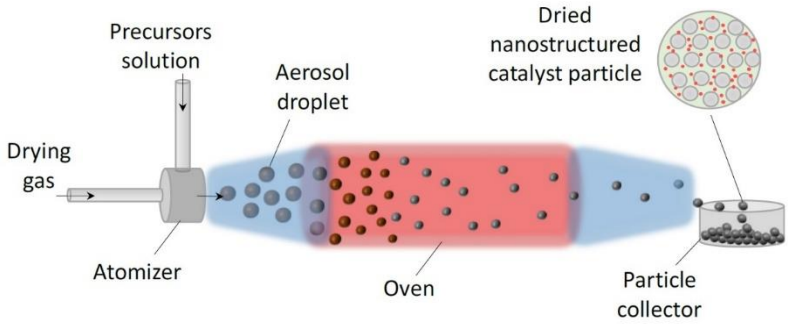


Figure 4. Schematic view of the AASG process that can be operated in a continuous mode for the one-pot production of nanostructured catalysts. The precursor solution contains a solvent, metal precursors, and a templating agent (e.g., a surfactant that will form micelles via evaporation-induced self-assembly, EISA). The droplets formed by atomization are transported in a drying gas towards a drying zone where the formation of structured particles takes place. Reprinted with permission from ref. [121]. Copyright 2020 Wiley.

Varied from the traditional way to stabilize the structure of Cu/ZnO catalyst, the compositions, sizes, and geometries of colloidal ZnO and Cu were tuned by the adoption of phosphinate ligands during synthesis [113]. As a result, the structure of the Cu and ZnO catalyst was stabilized whilst keeping the surface activity, providing a simple manner to regulate the stability and activity of the catalyst. In addition, the particle size, surface area of Cu, and the strongly basic sites in the Cu/Zn/Al/Zr compound were tuned by the incorporation of different amounts of fluorine (F) ions [109]. With such an approach, the activity and methanol selectivity can be systematically studied as a function of F content. An optimized result was obtained with F/Al = 0.83, where both the methanol yield and methanol selectivity reach the maximum.

The activity of the catalyst is sensitive to the microstructure and morphology. Yang et al. have prepared a $Cu/ZnO@m\text{-}SiO_2$ catalyst with a core–shell structure. The mesoporous pore of silica confined the size of Cu nanoparticles to a narrow size distribution at around 5 nm, which enables excellent stability against aggregation and deactivation, as well as superior catalytic activity [124], in line with the experimental findings by van den

Berg [131]. Additionally, highly dispersed Cu/graphene catalysts were obtained by the adoption of metal–organic frameworks (MOFs) template, showing nice CO_2 hydrogenation activity. This was achieved by introducing MOFs (e.g., HKUST-1) agent into the graphene layers, followed by high-temperature calcination. The ordered structure of MOFs enables the periodic arrangement of Cu nanoparticles, and the sequent pyrolysis of MOF further promotes the formation of ultrafine metal nanoparticles [123].

2.1.2. Role of Supports

The role of supports was originally thought to provide a carrier for well-dispersed metal particles and structural separation against sintering [97,132]. However, the SMSI effect was intensively reported in many supported catalysts having a strong influence on the chemical state, morphology, stability, activity, etc., of the catalysts [132,133]. For CO_2 hydrogenation to methanol catalysts, the frequently studied supports were ZnO [98,103], Al_2O_3 [97,134], ZrO_2 [118], CeO_2 [117,130], SiO_2 [124], and their mixed oxides [115,135].

For Cu/ZnO catalysts, the deactivation was proposed to follow the oxidation of Cu^0 to Cu^{2+} and the agglomeration of ZnO species [136]. To prevent the possible deactivation, measures must be adopted to stabilize the structure of ZnO and the oxidation state of copper, which can be achieved by either regulation of the structural promoter or the addition of a hydrophobic promoter. Other problems of the Cu-based catalyst are the sintering of the Cu component during reaction due to the relatively low Hüttig temperature (407 K) [137,138] and adsorbate-induced dynamic shape changes [139,140]. In this case, Al_2O_3 was usually adopted as a structural promoter to elevate the stability, as well as the dispersion of active components [138,141]. Comparatively, ZrO_2 appears to work in multiple ways [142]. A parallel comparison of Cu supported on CeO_2, ZnO, and ZrO_2 showed that the SMSI between Cu and CeO_2 leads to efficient dispersion of CuO and sufficient oxygen vacancies on the oxide support that stabilizes the intermediates (e.g., formate and methoxide) to produce methanol [117]. High coverage of formate species inhibits the RWGS reaction and therefore results in a high methanol selectivity [68]. Besides the SMSI effect, the apparent interactions between nitrogen species and Cu species have some impact on the microstructure of the resulted catalyst. As a result, the Cu-ZrO_2 catalyst supported on N-doped carbon nanotubes (CNTs) exhibits enhanced CuO dispersion that consequently promotes the reduction of Cu and hence the catalytic performance [118].

In addition, because of the good thermal stability and flexibly controlled microstructure, spinel structure materials have attracted research interest to tune the properties of Cu-based catalysts for methanol synthesis [135,143–145]. For Cu supported on $ZnFe_2O_4$ spinel catalyst, the size of Cu nanoparticles was adjustable according to the Cu/Zn and Zn/Fe molar ratios. Compared with the other Cu/ZnM-0.5 (M = Co, Ni, Sn, Cr, Al, Ga, and Mn) catalysts prepared with the same procedures, Cu/ZnFe-0.5 exhibits better methanol synthesis performance. The optimized 33Cu/ZnFe-0.5 catalyst exhibits a high methanol selectivity of 71.6% and a CO_2 conversion of 9.4% at 260 °C and 4.5 MPa. Therein, the spinel structure of $ZnFe_2O_4$ was thought to tune the formation of small ZnO adjacent to surface Cu NPs as well as the SMSI. The ZnFe spinel structure enhances the adsorption of CO and inhibits the weak and medium-strong CO_2 adsorption, resulting in improved methanol selectivity. The spinel structure catalysts, however, usually have relatively low surface area because of the high calcination temperature during preparation [135]. Combined with the microwave–hydrothermal synthesis method [116,135], a $Cu_{1-x}Zn_xAl_2O_4$ precursor with a high specific surface area was obtained. Thanks to the separation of the spinel lattice, very small Cu particles (<4 nm) were obtained with the exposed Cu surface area of 8 m^2/g. The catalyst also exhibited good structural stability against aggregation in the following reduction process. Similarly, tuning of the microstructure and intrinsic catalytic properties of $Cu/ZnAl_2O_4$ was also achieved by adding Cr or Ga [145].

2.1.3. Promoters

The effect of the promoter in the heterogeneous catalyst is structural and electronic in nature [146,147]. For instance, superior methanol selectivity has been achieved by potassium (K) promoted Cu-Zn-Al catalyst (CZA-K) [87]. Compared with sodium (Na), the Cu^+/Cu ratio of CZA-K is higher, which enables better CO_2 hydrogenation activity. The formation of surface K-O-(CO)-O species prevents the dissociation of CO_2, leading to a limited RWGS reaction and higher methanol selectivity. Ga_2O_3 added to Cu-ZnO/HZSM-5-based catalyst can effectively increase the specific surface area, reduce the size of the metallic component and maintain a relatively high Cu^+ content, all of which were thought crucial for the hydrogenation of CO_2 [148]. Besides, indium (In) shows a good promotion effect for Cu/CeO_2 catalyst. Loading of 1 wt% indium in Cu/CeO_2 leads to a prominent improvement in methanol yield rate. The promotion effect herein includes smaller Cu particle size and improved dispersion and stability of Cu [119].

With a surface organometallic chemistry (SOMC) approach, Cu supported on SiO_2 with different promoters (Ti, Zr, Hf, Nb, Ta) was successively prepared. Importantly, the prepared catalysts have the same physicochemical properties, in which condition the role of the promoter can be compared in parallel. As the promoters were proposed to modify the Lewis acid strength of interfacial metal sites [120] that correlates with the stability of the reaction intermediates (formate and methoxy) at the periphery of Cu nanoparticles, a promoter with stronger Lewis acid metal sites will enable a better catalytic activity over Cu-based catalyst.

In addition to the exotic promoters, it was also reported that the methanol itself may act as a promoter over Cu/ZnO/MgO catalyst. With the presence of a small amount of methanol in the reactant steam, the apparent activation barrier was notably reduced (from 117.9 kJ/mol to 67.9 kJ/mol) [149]. The origin of the methanol promotion effect was not discussed in the publication but is possibly related to the interaction between methanol and the catalyst with the self-limiting activity expected.

2.2. In_2O_3-Based Catalysts

In_2O_3 was initially reported to show excellent catalytic activity for methanol steam reforming with extremely high selectivity of CO_2 relative to that of Cu/ZnO catalysts [150]. In 2012, Ge's group published a theoretical paper predicting the methanol synthesis activity of In_2O_3 from CO_2 hydrogenation [151]. In the following paper, oxygen vacancy (D4) was deemed to play a key role in the activation of CO_2 and stabilizing the key intermediates involved (see Figure 5 for the structure of ideal and defective In_2O_3(110) surface) [42]. Since then, a number of works have been published reporting the superior activities and selectivities of pure In_2O_3 or In_2O_3-based catalysts [83,152–161]. A very early experimental test was performed on commercial In_2O_3 powders after simple calcination in air at 500 °C for 5 h [158]. The catalyst showed somewhat comparable activities with the reported Cu-based catalysts. This could be a promising result since only pure In_2O_3 was applied, not to mention the unknown specific surface area.

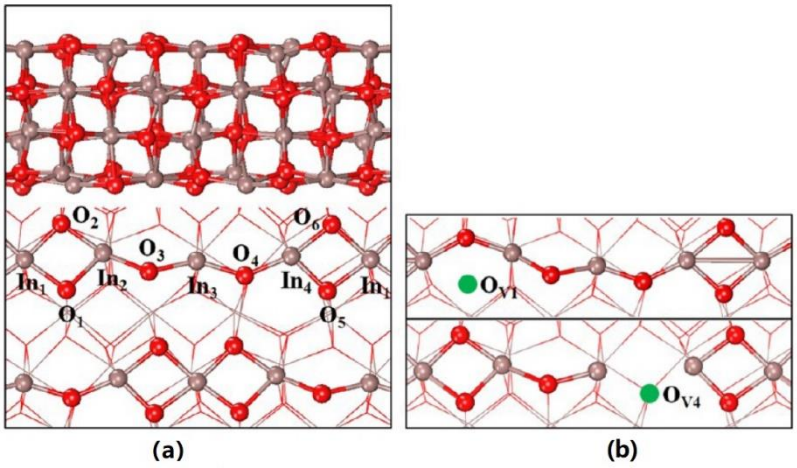


Figure 5. (**a**) Optimized structure of the In_2O_3(110) surface, side view (upper), and top view (lower). (**b**) The D1 (upper) and D4 (lower). Reprinted with permission from ref. [42]. Copyright 2013 American Chemical Society.

Various strategies have been adopted to improve the performance, including: (1) noble metal loading to facilitate H_2 activation and formation of oxygen vacancies; (2) introduction of oxide support to elevate the dispersion and resist sintering of the active component; (3) adoption of different synthesis methods to achieve novel morphological, electronic, or interfacial effects.

Recently, Liu's group has reported an In_2O_3 supported Ir catalyst (Ir/In_2O_3) showing enhanced activity, methanol selectivity as well as stability under the reaction condition of 300 °C, 5 MPa, and 2100 h^{-1} while keeping the H_2/CO_2 ratio of 4 [83]. The catalyst was prepared by precipitation and impregnation method giving a specific surface area of 68 m^2/g. Therein, the interaction between Ir and In_2O_3 has proposed the key role in determining the structural characteristics of the catalyst, including a high dispersion of Ir, avoidance of over-reduction of In_2O_3, and stabilized oxygen vacancies that were thought to be the activation center for CO_2 molecules. Similarly, Rh supported on In_2O_3 prepared by the deposition–precipitation method also exhibited good activity (space-time yield (STY) of methanol up to 0.5448 $g_{MeOH} \cdot g_{cat}^{-1} h^{-1}$) and selectivity (56.1%) for CO_2 hydrogenation to produce methanol [16]. Higher selectivity was achieved at a lower reaction temperature due to the unfavorable RWGS at a lower temperature. The introduction of Rh gives rise to an enhanced H_2 dissociation efficiency, and the sequent spillover to In_2O_3 further promotes the formation of surface oxygen vacancies. Similar effects were also found for Ni, Pt, Rh, Au, and Ru supported on In_2O_3 [16,80,83,155,156,159,161].

Supported catalysts, however, sometimes suffered from sintering even though the metal nanoparticles were separated physically by support materials [136,152]. Appropriate interaction between support materials and metal nanoparticles may hinder the sintering to some extent. Au/In_2O_3 catalyst prepared by deposition–precipitation method has exhibited the consequence of the interactions [80]. The Au/In_2O_3 catalyst yields a methanol selectivity of 67.8% with the STY of 0.47 $g_{MeOH} \cdot g_{cat}^{-1} h^{-1}$. After a 12 h on-stream test, the conversion of CO_2 dropped by only 0.5%, and the mean particle size of the Au nanoparticles was slightly changed from 1.0 nm to 1.3 nm, indicating a nice structural stability that was not seen on other oxide support [80,157]. In addition, anchoring of Pd to the lattice of In_2O_3 leads to superior catalytic performance, as well as structural stability. By controlled coprecipitation, Pd was atomically dispersed in the lattice matrix of In_2O_3, and the growing up of the Pd cluster was efficiently hindered [152].

Another challenge of the In_2O_3 catalysts for CO_2 hydrogenation is the structural instability of In_2O_3 during reaction [160], which can be overcome by choosing appropriate support materials [78,79]. Using ZIF-67(Co) MOFs as precursors, Pustovarenko et al. successively synthesized Co_3O_4-supported In_2O_3 composites (In_2O_3@Co_3O_4) [78]. After ZIF-

67(Co) was synthesized, it was impregnated with aqueous indium nitrate solution and then dried under vacuum and calcined under different thermal conditions (including pyrolysis at 600 °C in nitrogen flow and calcination at 400 °C in airflow). The obtained 3In@4Co(20) catalyst showed methanol selectivity of 75%, CO_2 conversion of 17.3% and methanol STY of 0.65 $g_{MeOH} \cdot g_{cat}^{-1} h^{-1}$ at 285 °C, 50 bar and gas hourly space velocity (GHSV) = 15,600 h^{-1} with H_2/CO_2 = 4:1. On the one hand, the In distribution all over the metal-organic matrix, micropore, and interparticle surface area can be optimized through tuning the textural properties of ZIF-67(Co); on the other hand, the formation of mixed metal carbide, namely $Co_3InC_{0.75}$, formed during the pyrolysis–calcination process can effectively stabilize high dopant distribution and prevent the formation of large oxide domains, which is beneficial to shorten the induction time during CO_2 hydrogenation.

Martin et al. [79] compared the performance of pure In_2O_3, In_2O_3 supported on monoclinic ZrO_2 (In_2O_3/m-ZrO_2) and Cu/ZnO/Al_2O_3. 100% methanol selectivity was achieved under industrial conditions (T = 473–573 K, P = 5.0 MPa, GHSV = 16,000 h^{-1}) over the pure In_2O_3 (Figure 6). The STY of methanol varies with reaction temperature as well as the CO concentration in the feed (keeping H_2/CO_2 = 4:1) (Figure 6), which was ascribed to the evolution of oxygen vacancies. By comparison, the In_2O_3 supported on monoclinic ZrO_2 significantly improves the yields of methanol because of the promoted formation of oxygen vacancies, the better dispersion of In_2O_3, the resistance against sintering, and possibly the modulation of the In_2O_3 activities by a catalyst–support interactions. In addition, the supported In_2O_3 showed excellent stability over 1000 h under reaction conditions. For both In_2O_3 and In_2O_3/ZrO_2, the oxygen vacancies were emphasized to play a key role in the adsorption and hydrogenation of CO_2 molecules.

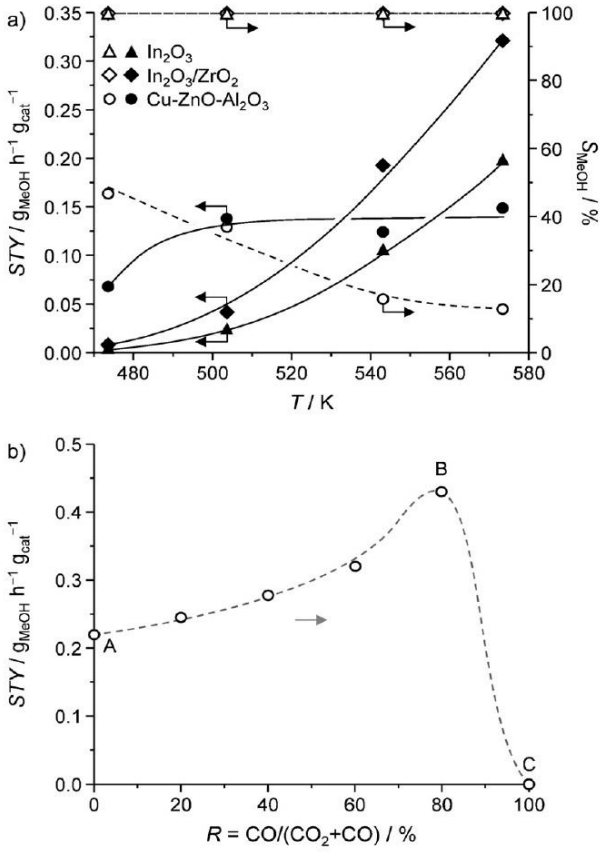


Figure 6. (**a**) Methanol STY and selectivity for CO_2 hydrogenation over bulk In_2O_3, In_2O_3/ZrO_2 (9 wt% In), and the benchmark Cu-ZnO-Al_2O_3 catalyst at various temperatures. (**b**) Methanol STY over bulk In_2O_3 as a function of the CO concentration in the feed at 573 K. Reaction conditions: p = 5.0 MPa, H_2/CO_2 = 4:1, and GHSV = 16,000 h^{-1}. Reprinted with permission from [79]. Copyright 2016 Wiley.

To further understand the role of ZrO_2 support, Frei et al. have prepared a series of In-Zr mix-oxide (synthesized by coprecipitation method with the molar content of In from 0 to 100%) and supported In_2O_3 catalysts (on monoclinic and tetragonal ZrO_2 by wet impregnation method) [162]. The mix-oxide showed strong electronic interaction between In_2O_3 and ZrO_2 while displaying inferior CO_2 hydrogenation activity, indicating a negligible electronic contribution of ZrO_2 to the activity enhancement. For supported catalysts, however, the methanol yield was about one order higher for In_2O_3 supported on m-ZrO_2 than that on t-ZrO_2, although on both supports, nuclear magnetic resonance (NMR) results showed ordered fine epitaxial In_2O_3. The ultraviolet–visible (UV-vis) spectrum of In_2O_3/m-ZrO_2 shows more absorption in the band gap, indicating a higher density of oxygen vacancies in the oxide. The m-ZrO_2 and t-ZrO_2 are slightly different in lattice constant, which makes the lattice mismatch to In_2O_3 of 1.2% and 0.5%, respectively. The slightly larger lattice mismatch between In_2O_3 and m-ZrO_2 tends to generate tensile strain that favors the formation of more and possibly diverse oxygen vacancies on In_2O_3 [154,162]. The large discrepancy in catalytic activity was also attributed to the formation of electron-rich In_2O_3 because of the electron transfer from ZrO_2 to In_2O_3 [163], which could be from the same origin. The work highlighted the role of imperfect epitaxy in the formation of vacancies (defects) and consequent catalytic activities. Also, one must note that the peculiarity of m-ZrO_2 over t-ZrO_2, in this case, cannot be simply transplanted to other systems, e.g., Cu, Ag, and Au supported on t-ZrO_2 were reported to show either better [164,165] or worse [166] CO_2 hydrogenation performance than on m-ZrO_2, depending on the preparation method and pretreatment conditions. Further modification of In_2O_3/ZrO_2 system was achieved by loading active metals, e.g., via a coprecipitation method to obtain Au/In_2O_3-ZrO_2 catalysts [84]. While the Au nanoparticles (NPs) in the solid solution facilitate H_2 dissociation, the presence of Zr stabilizes the structure of In_2O_3 and increases the number of oxygen vacancies, both as the result of SMSI.

Indeed, the SMSI between Pd and In_2O_3 may lead to a bimetallic species that causes weakening of H_2 dissociation ability and hence the attenuation of the catalytic activities [167]. To avoid such alloy formation, Liu's group prepared the supported catalysts by introducing Pd-peptide composite, followed by a thermal treatment [168]. Compared with the conventionally prepared supported catalyst by the impregnation method, the resulted catalysts showed much better metal dispersion with a mean particle size of 3.6 nm and improved catalytic activities. The author attributed the improved performance of Pd-P/In_2O_3 catalysts to the enhanced H_2 activation and more pronounced CO_2 adsorption ability as the result of highly dispersed Pt nanoparticles and the interfacial effect associated with the preparation method. In addition, atomically dispersed Pt/In_2O_3 [169] was also reported to show good stability due to the higher barrier against sintering. A small amount of Pt loading (0.03–0.58 wt%) by coprecipitation results in anatomically dispersed doping of Pt in the In_2O_3 lattice. The Pt^{n+}, though part of which is initially sintered under reaction conditions, facilitates the formation of oxygen vacancies and also the activation of hydrogen molecules.

2.3. Nanoalloy Catalysts

Nanoalloy catalysts often exhibit unique electronic structures distinguished from either component [106,170–172]. As a result, the bonding properties of reactants, intermediates, or products can be tuned, which finally yields tunable activity and selectivity of the catalysts. Nanoalloy is formed either in the preparation process or under reaction conditions. The existence of nanoalloy can be validated by the finger-printed diffraction angle (2θ) in X-ray diffraction (XRD) [173], the alloy state of an element in X-ray photoelectron spectroscopy (XPS) [174], the specific vibrational mode of probe molecules binding to the alloy sites [175], or the lattice constant value shown in transmission electron microscopy (TEM) [88,176]. For a specific reaction, the turnover frequency (TOF) can be tuned by either the composition or the relative content [177]. Studt et al. compared the catalytic activities of three Ni-Ga catalysts via incipient wetness impregnation method and

$Cu/ZnO/Al_2O_3$ catalyst via coprecipitation route as reference [102,177]. The better activity and methanol selectivity of the Ni_5Ga_3/SiO_2 catalyst were attributed to the suppressed RWGS activity. While supported on mesoporous nitrogen-rich carbon, Ni_5Ga_3 was also found to have good activity for CO_2 hydrogenation, though the activity is sensitive to the preparation method [176]. The author highlighted the freeze drying method that enables uniformly distributed metal nanoparticles with an average size of 2–5 nm and correlated the formation of NiGa alloy with the suitable local environment realized by the preparation method.

Shi et al. [88] synthesized Cu-In intermetallic catalyst and investigated the effect of reduction temperature on the reaction activity. It was found that reduction temperature exerts a notable influence on the formation of alloy, the crystallite size, and the adsorption of gases. For instance, CuO was reduced to metallic Cu at 250 °C, and the $Cu_{11}In_9$ alloy appeared when the reduction temperature was above 300 °C. With higher reduction temperature, the crystallite size of $Cu_{11}In_9$ increases slightly, accompanied by an attenuated H_2 adsorption ability. The CO_2 adsorption ability varies notably with increasing the reduction temperature, and the maximum value was obtained with CuIn-300 (reduced at 300 °C), the trend of which agrees well with the STY of methanol tested at 240 °C and 3 MPa (for the same reason, the CO_2 adsorption ability was thought to be the key factor for the design of Cu/In_2O_3 catalysts). Besides the temperature, reduction pressure also affects the formation of alloy. An X-ray absorption near edge structure (XANES) analysis on the reduction process of commercially available $Cu/ZnO/Al_2O_3$ catalyst at different pressure (1 mbar–10 bar) showed that Cu–Zn alloys were formed only under reduction pressure of 100 mbar or above [178]. The maximum reduction rate (simultaneous formation of copper (0)) is gradually shifted to low temperature by elevating the reduction pressure. The catalysts started to show methanol synthesis activity when the total pressure was above 1 bar, along with the increased formation of oxygen vacancies and other structural distortions in the ZnO phase.

Note that, in this section, we do not really attempt to emphasize the alloy formation in the activity modification for the metal supported on oxide since their interactions are not necessarily accompanied by the formation of nanoalloy. For Ni supported on In_2O_3, the authors emphasized the role of Ni–In alloy formation in determining its activity [153,172], while Hensen and coworkers [179] claimed the activity of Ni/In_2O_3 system stems from the synergy effect with no alloy formation evidenced. In any case, the formation of nanoalloy in modifying the electronic structure and hence the catalytic performance provides a novel idea for catalyst design.

2.4. Other Catalysts

MoS_2 and MoS_2-based materials have been widely used as lubricants [180], transistors [181], heterogeneous catalysts [182–184], and gas sensors [185]. Due to the special lattice structure, MoS_2 is easily peeled into thin layers or even a single atomic layer [186]. The electronic structure of two-dimensional MoS_2 is sensitive to the status of surface vacancies. The sulfur (S) vacancies especially located at edges or in-plane, exhibit completely different catalytic activities [90,187,188]. The edge S vacancies were thought to catalyze the CO_2 hydrogenation to methane, while the in-plane S vacancies were proven to be ideal active sites for CO_2 hydrogenation to methanol [90]. Over the in-plane sulfur vacancy-rich MoS_2 nanosheets, a methanol selectivity of 94.3% at a CO_2 conversion of 12.5% was achieved at 180 °C, and the catalyst was stable for over 3000 h without any deactivation. The findings enlightened the potential role of the in-plane vacancies in catalysis, and further modification of the vacancies-controllable MoS_2 material or two-dimensional material is meaningful.

Due to the unique structural characteristics, MOF materials were featured with highly ordered and tunable porous structures, high surface area, flexible organic linkers, and metal centers [189–191]. Accordingly, MOFs can be a template for porous material

synthesis [123], supporting materials for nanocatalysts [191,192], or act as catalysts individually by introducing active metal centers as nodes or located on the MOF linkers [193,194], as shown in Figure 7. Although many MOFs suffer from high temperature and moisture conditions, some selected MOF-based catalysts, including UiO-bpy [191], MOF-74 [192], UiO-67 [194], and UiO-66 [195], were reported to have good thermal stability even under moisture condition, of which further tuning of the catalytic properties is likely foreseen.

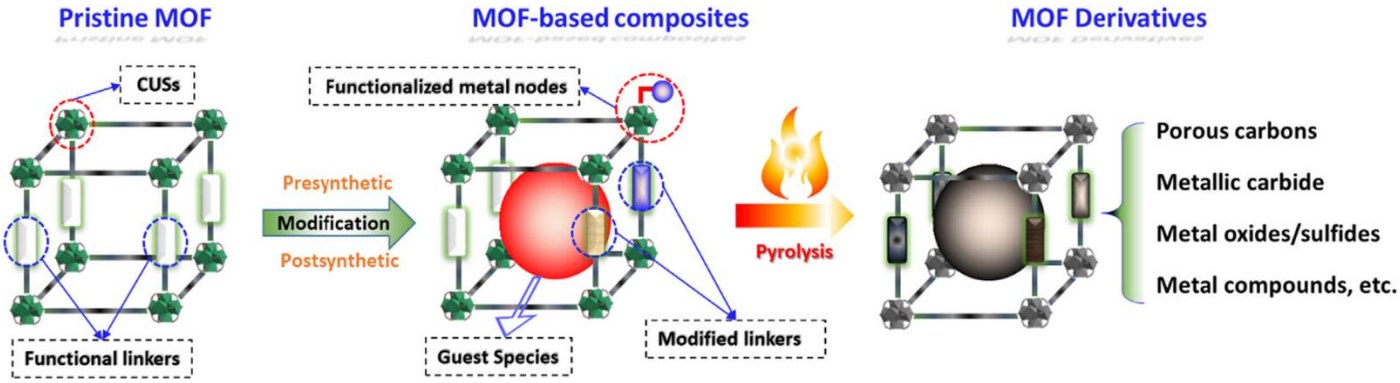


Figure 7. Schematic representation of the catalytic site locations on/in different types of MOF-based catalysts. Reprinted with permission from ref. [189]. Copyright 2019 Elsevier.

Another promising catalyst catalog for CO_2 hydrogenation to methanol is solid solution catalysts [74,196–198]. Wang et al. have prepared a series of ZnO-ZrO_2 solid solution catalysts through the coprecipitation method [196]. Both methanol selectivity and CO_2 conversion reach maximum over the catalyst when Zn/(Zn + Zr) ratio is around 13%. Methanol selectivity of 86% to 91% with CO_2 conversion of 10% was achieved under the condition of 5.0 MPa, 24,000 $mL \cdot g^{-1}h^{-1}$ and 320 °C. The catalyst was proved to show long-term thermal and chemical stabilities against sintering and poisoning by, e.g., SO_2 or H_2S. Density functional theory (DFT) simulation results suggested that Zn and Zr provide the adsorption sites for H_2 and CO_2, respectively. Therefore, a solid solution catalyst takes advantage of both components to achieve the synergetic effect. Such synergetic effect was also observed in other solid solution catalysts such as M_aZrO_x (Ma = Cd, Ga) [197]. Another interesting aspect of the ZnO-ZrO_2 solid solution catalyst is that its activity was reported to be sensitive to the preparation method (the microstructure) rather than the ZnO/ZrO_2 ratio. The 20% ZnO-ZrO_2 catalyst prepared by the evaporation-induced self-assembly process exhibited better methanol synthesis activity than that of the coprecipitation method [74]. The enhanced activity of the former was ascribed to its larger specific surface area related to the mesoporous structure and more active sites for CO_2 and H_2 adsorption (which are possibly correlated with the larger surface area).

3. Mechanistic Understanding

As shown in the above text, large numbers of catalysts have been reported on their superior activities for CO_2 hydrogenation to methanol. They may be synthesized with different methods, from different sorts and proportions of raw materials, treated with different parameters, or activated under different reaction conditions. Consequently, the resulted catalysts are featured with varied compositions (at surface region), microscopic morphologies, particle sizes, surface area, bonding properties, etc., finally leading to unique activity, selectivity, and stability. One of the practically noticeable consequences is the gradually improved STY and methanol selectivity in the newest publications. Parallel to the improvement in catalyst development, a comprehensive understanding of the structure–activity relationship has made a lot of progress based on systematic kinetic analysis, surface science study, operando techniques, theoretical simulations, etc., although

one must note that some reported mechanisms might be case-dependent and not expanded to other systems.

An active site is one of the most important concepts in the study of catalysis [199–201]. It functions in multiway, providing adsorption sites for reactants, diffusion routes for adsorbate, suitable microscopic geometric matching for the reaction, appropriate bonding to intermediates, etc. Therefore, an active site is generally not a single point, a special micro or macrostructure, or a certain element with a specified chemical state, but the combination of a series of microscopic locations with distinctive functions and special elemental, electronic and geometric matching for the certain specific catalytic reaction [201]. It is an arduous task to build up a panorama of an active site, not to mention the difficulties superimposed by the structural complexity of nano-sized particles and numerous interferential issues. An alternative and feasible way is to simplify the catalyst system, e.g., to perform reactions on structurally well-defined model catalysts, such as single crystals, polycrystalline, and thin films [202–204]. In this section, we summarize the works about active sites for catalytic hydrogenation of CO_2 to CH_3OH on both modeled single crystals and realistic powder catalysts.

3.1. The Chemical State of Copper

As early as the 1990s, Goodman et al. [205] have studied the hydrogenation of CO_2 to CH_3OH over Cu(100) surface under the condition of 500–550 K and 44–102 kPa, with the feed composition of $CO_2/CO/H_2$ being 1/2/12. The activation energy of CO_2 hydrogenation to CH_3OH was estimated to be 73.4 ± 6.0 kJ/mol. No metallic copper was detected after the reaction, indicating that copper may take effect in an ionic state. They, therefore, concluded that CO_2 only plays a positive role in keeping the copper in a suitable oxidation state, and CO provides the carbon source for the reaction. In contrast, Chorkendorff et al. [206] worked on the hydrogenation of pure CO_2 on Cu(100) under the reaction conditions of 543 K and 2 bar (CO_2/H_2 = 1:1) and did not find the oxidized state of copper after the reaction. However, they obtained similar apparent activation energy of 69 ± 4 kJ/mol. The introduction of CO into the reaction system significantly enhanced the reactivity by lowering the reduction barrier, where CO was thought not to participate in the reaction [171,207]. The discrepancy in the carbon source was likely unified by a DFT and kinetic Monte Carlo (KMC) study [208], which revealed that the main carbon source on the Cu(111) (metallic Cu) surface is CO_2, whereas on Cu_2O(111) (ionic Cu) surface is CO.

Besides the chemical state, CO_2 hydrogenation to CH_3OH is also sensitive to the coordination state of copper. Compared with Cu(100) [205] and polycrystalline Cu foil [209], Cu(110) [210] exhibits higher CO_2 hydrogenation activity in its metallic state. The apparent activation energy for the synthesis of CH_3OH on Cu(110) was measured to be about 67 kJ/mol, close to that on Cu(100) [205] and polycrystalline Cu foil (77 ± 10 kJ/mol) [209]. However, the apparent activation energy for RWGS on Cu(110) was measured to be 78 ± 14 kJ/mol, which is significantly smaller than that on polycrystalline Cu (135 ± 5 kJ/mol) [209]. Likewise, not all surface Cu atoms are active in the reaction. DFT results of CO_2 adsorption over Cu(100) surface have shown that CO_2 only dissociates at step sites [32]. While Kim et al. [211] found that the dissociation occurs only when H_2 is coadsorbed on step sites, where CO_2 is activated and converted to CO, surface oxygen (O*), and surface hydroxyl (HO*). Moreover, these active species were subsequently converted into carbonate (CO_3^{2-}), bicarbonate (HCO_3^-), and formate (HCOO*) species. Formate species formed on terrace sites were then converted to CH_2O(O) on step sites that were subsequently converted to methoxy and methanol.

In numerous cases, the phase and microstructure are varied dynamically with the ambient environment, such as pressure, temperature, proportion, duration, etc., making the determination of the active site unconvincing. In such a situation, in situ or operando spectroscopic investigation may tell some more detailed information [212,213]. Ren et al. [214] provided direct spectroscopic evidence for the microscopic process of CO_2 hydrogenation to CH_3OH on Cu(111) surface at room temperature by near ambient pressure X-

ray photoelectron spectroscopy (NAP-XPS), ultraviolet photoelectron spectroscopy (UPS), and low energy electron diffraction (LEED). They found that CO_2 dissociates on Cu(111) surface to form atomic oxygen, and hence Cu-O species under CO_2 + H_2 atmosphere, which consequently promote CO_2 hydrogenation to CH_3OH through formate pathways, as shown in Figure 8.

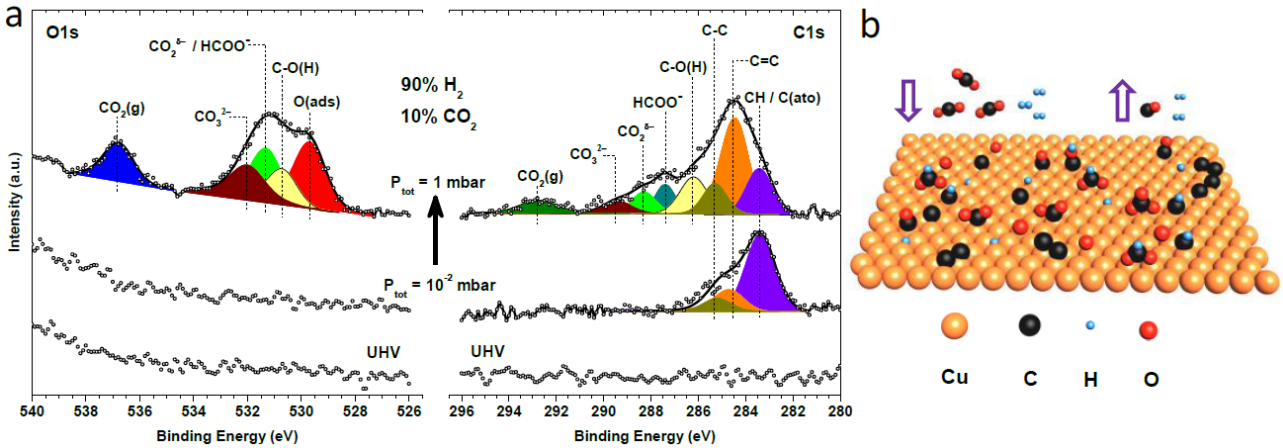


Figure 8. The schematic of catalytic hydrogenation of CO_2 to CH_3OH on Cu(111) surface. (**a**) NAP-XPS spectra of C 1s (right) and O 1s (left). All spectra were obtained at fixed CO_2 and H_2 ratio ($P(CO_2)/P(H_2)$ = 1/9) and a total pressure of ultrahigh vacuum (UHV) (lower panel), 10^{-2} mbar (middle panel), and 1mbar (upper panel), respectively. (**b**) The schematic illustration. Reprinted with permission from ref. [214]. Copyright 2018 Wiley.

3.2. Strong Metal–Support Interaction

The concept of strong metal–support interaction (SMSI) was initially put forward to explain the attenuated adsorption ability (e.g., to CO and H_2) of the group VIII metals supported on TiO_2 after reduction at high temperature (e.g., 500 °C) [215]. The concept was extended to metal particles supported on reducible transition metals. Even more generally, the support materials were believed not to be limited to transitional or reducible if the surface reduction actually occurs (e.g., the oxides of niobium, manganese, and lanthanum) [216,217]. Later, the SMSI effect was also observed under oxidative treatment conditions, further extending the generality of the concept [218]. Although the driving force for SMSI is energetic in nature, it is often accompanied by electron transfer between metal and support, formation of an intermetallic bond, coating of metal by support or of support by metal, and behaviors related to them (e.g., formation of oxygen vacancies, presence of interface and synergetic effect, stabilization of metal component against thermal and chemical sintering, tunable bonding properties of the catalyst, etc.). Herein, one must note that the consequences induced by SMSI are not necessarily positive for catalytic properties, just like the case it came from, but provide the possibility to tune the properties of catalysts.

For the industrially available $Cu/ZnO/Al_2O_3$ catalyst, it is generally agreed that ZnO acts as either support to separate Cu nanoparticles physically or an electronic and structural promoter to give rise to synergy effect with the latter mainly induced by SMSI [133,215]. The effect of SMSI may include the formation of the positively charged metal component, oxygen vacancies (with different types), Cu–Zn alloy, electronic doping of ZnO, and possibly the consequent stabilization of copper nanoparticles and metal–oxide interfaces [98,106,108,219]. A direct demonstration of the SMSI effect on catalytic activity was carried out by Behrens et al. [98], where Cu steps were thought to be one of the key factors to facilitate the formation of methanol. The presence of $Zn^{\delta+}$ at defect sites was verified to be the result of the dynamic SMSI effect leading to the partially covered metal particles with ZnO_x. The dynamic change was also accompanied by the alloy formation

through substitution of Zn into the Cu steps, the presence of partially oxidized $Zn^{\delta+}$, and the geometric matching between Cu steps and adjacent ZnO_x for stabilizing the intermediates to methanol.

Fujitani et al. [220] have studied the influence of Zn deposition on the activity of Cu at 523 K and 18 atm and found that moderate coverage of Zn could promote the methanol synthesis of Cu(111) while poisoning the Cu(110). The promotion effect of Zn on Cu(111) was ascribed to the preferential formation of ZnO_x species on Cu(111) over Cu(110) surface. This could be indirect evidence to show the effect of SMSI on the activities of Cu/ZnO catalysts. A further study by Nakamura et al. [221] showed that Cu^+-O-Zn species are formed during CO_2 hydrogenation over polycrystalline Cu surface with Zn deposition. The presence of Cu^+-O-Zn species stabilizes the intermediate species (formate and methoxy). On the physically mixed Cu/SiO_2 and ZnO/SiO_2 powder catalysts [222], they also found that ZnO moiety partly migrates onto the Cu surface, creating Cu^+-O-Zn active species and partly dissolves into Cu particles to form Cu–Zn alloys. After deposition of Cu clusters on ZnO(0001)-Zn terminated surface, a small amount of Cu promoted the reduction of ZnO by triangular reconstruction for syngas hydrogenation to CH_3OH [223]. The metallic zinc leads to the formation of Cu–Zn alloys, which exhibit an excellent activity for CH_3OH formation.

3.3. Interfacial Effect

The Cu–ZnO interface was believed to be a key factor for Cu/ZnO catalysts, which has been evidenced by the metastable "graphite-like" ZnO_x layers on the top of Cu nanoparticles observed by transmission electron microscopy (TEM) [126]. Palomino et al. [224] also found that the reactivity of Cu single crystal surfaces was significantly enhanced after the deposition of ZnO nanoparticles. The activity follows Cu(111) < Cu(100) < ZnO/Cu(111) < ZnO/Cu(100), where the role of Zn was thought to stabilize the formate intermediate. Kattel et al. [103] have compared the activity of Zn–Cu alloy and ZnO/Cu model catalysts for methanol synthesis and found that metallic zinc nanoparticles were transformed to ZnO after running CO_2 hydrogenation reaction over the Zn/Cu(111) catalyst at 525 K and 550 K. They, therefore, concluded that the synergy of ZnO and Cu at interface catalyze the hydrogenation of CO_2, although Nakamura et al. thought the positive valence state of Zn after reaction could be the result of formate species binding to Zn [104,173,105].

Despite the unsettled divergence in the XPS assignment, the model proposed by Muhler et al. [125] about the structural change over time on stream (TOS) possibly provided a unified understanding (Figure 9). The Zn–Cu alloy was initially formed during the reduction process on Cu/ZnO prepared either by coprecipitation method [225] or by a physical mixture of Cu/SiO_2 and ZnO/SiO_2 [221]. The Zn species was then partially oxidized to $Zn^{\delta+}$ at the defective Cu sites under CO_2 hydrogenation conditions due to the SMSI effect [103,104]; Along with diffusion and oxidation of Zn, there may form a graphitic-like ZnO_x layer on Cu [126,226,227]; and finally, thick ZnO layers are formed after long-term reaction under CO_2 hydrogenation conditions [228]. In the whole process, the initial fast-decreased activity was thought to be the result of the partial restructuring of ZnO, which influences the stability of the Cu–ZnO interface; the long-term deactivation was ascribed to the loss of specific surface and Cu–ZnO interface due to the crystallization of ZnO.

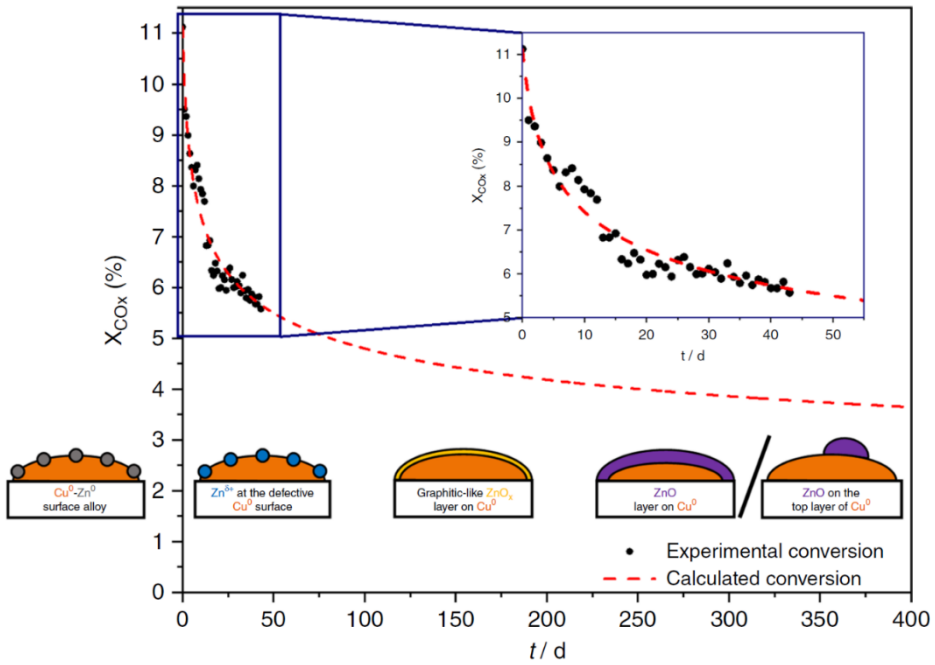


Figure 9. Long-term methanol synthesis over the industrial $Cu/ZnO/Al_2O_3$ catalyst at 210 °C and 60 bar. Recorded degrees of conversion (black points) under differential controlled conditions. The dashed red curve describes the intra and extrapolation of the experimental data, which were calculated with the MATLAB® software according to the studies of Fichtl et al. [229]. Illustrations from left to right: Cu^0–Zn^0 surface alloy according to Nakamura et al. [230]. $Zn^{\delta+}$ species at the defective Cu^0 surface according to Behrens et al. [98], graphitic-like ZnO_x layer on Cu^0 according to Lunkenbein et al. [126]. ZnO layer on Cu^0 according to Lunkenbein et al. [228] as well as Fichtl et al. [229] and ZnO on the top layer of Cu^0 according to Kattel et al. [103]. Reprinted with permission from ref. [125]. Copyright 2020 Springer.

The interface (or synergetic) effect of Zn–Cu alloy was predicted by DFT simulations as well, where Zn atoms are located on the Cu surface in the form of single atoms or clusters [231]. At the Cu–Zn interfaces, both single-atom Zn and Zn clusters (Zn_3) can catalyze CO_2 to methanol with the activation barrier notably lower than that on a pure Cu surface [232]. While the Zn single atom/Cu interface is thermodynamically and kinetically resistant to oxidation, the Zn clusters can be easily oxidized through the dissociation of CO_2 at interfaces (which is likely the case under industrial reaction conditions), leading to an obvious reduction of the reaction barrier. Similarly, the rate of methanol formation over CeO_x/Cu(111) was found about 200 times faster than that on Cu(111), which was ascribed to the synergetic effect of the interface between two complementary components of copper and ceria [233]. The ceria components stabilize CO_2^- and OH species, providing complementary chemical properties for Cu catalysts. Such unique matching was barely observed on pure Cu or Cu–Zn alloys [98,234], which emphasizes the uniqueness of the metal–oxide interface in property tuning. Such effect was also observed on Cu-CeO_2 [68], Pd-Ga_2O_3 [235], Au-CeO_x/TiO_2 [236], Cu/ZrO_2 [111,237], Cu/Al_2O_3 [128], CuO-In_2O_3 [88], Au_4/In_2O_3 [156], etc. Overall, the interfacial effect in supported catalysts is not only a geometric matching but also an electronic effect, just as the fact that it is often induced by SMSI.

3.4. Size Effect

In some earlier years, the size-dependent activity has been largely reported on gold and other catalysts [238,239]. The single-atom catalysts reported in recent decades could belong to the catalog as well. The size effect is mainly an electronic effect, with no exclusion of the possibility of structural effect since the convergence of surface energy may lead to different geometry and lattice parameters of the nanoparticles [240]. Pacchioni et al.

[241] have investigated the electronic structure of rutile TiO_2(110) thin films ranging from two to ten layers and observed oscillated band edges (bottom of conduction band (CB) and top of valence band (VB)) and varied band gaps. When reducing the particle size of metal clusters, the energy levels of the frontier electron orbitals become more localized, and loss of metallic properties may occur at some critical dimension. Che and Bennett [242] roughly estimated the size effect of metal particles by comparing the spacing of electronic levels of the particle with thermal energy kT and obtained the critical dimension of about 2 nm. Despite the unknown error bar, it gave a reasonable coincidence with the reported work where the physical and catalytic properties start to change near this dimension. Goodman and coworkers [239] have studied the size-dependent activity of Au/TiO_2 for CO oxidation and found the activity reaches the maximum at two-atom-thick clusters in which nonmetallic properties start to appear. The size dependency of Au activity was thought insensitive to the support materials [238,243].

For small Cu clusters (n = 3, 4, 20) supported on Al_2O_3 thin films, the catalysts exhibit strong size- and temperature-dependent activity for CH_3OH synthesis [244]. Cu_3/Al_2O_3 shows maximum activity at 175 °C, while Cu_{20}/Al_2O_3 is more active at higher temperatures (275–325 °C). For all temperatures tested, Cu_4/Al_2O_3 was the most active one. The finding differs from the quasi-linear relationship between methanol synthesis activity and specific Cu surface area for each class of the catalysts (e.g., Cu/ZnO, Cu/Al_2O_3, and $Cu/ZnO/Al_2O_3$) reported by Kurtz et al. [138]. The discrepancy is caused by the size effect, possibly through the change in electronic properties, since the Al_2O_3 is only a structural promoter in the Cu/Al_2O_3 catalyst (a synergetic effect is ruled out). Although the grouping of different catalysts proposed by Kurtz may not represent a general case, the work evidently exhibited that the size effect is not isolated but correlated with the microenvironment of the active components.

Zhang et al. [245] have worked on a series of Cu clusters with DFT simulations and observed a linear relationship between the CO_2 hydrogenation activity and the adsorption energies of CO and O on Cu clusters. The latter were thought to correlate with the location of the d band center that varies with the size of clusters. Note that the maximum cluster adopted in the calculations consisted of 79 Cu atoms which correspond to a diameter of about 1.5 nm. For large clusters, Karelovic et al. [246] claimed that the intrinsic activity for methanol synthesis is independent of the particle size (from 8.5 to 37.3 nm), and the enhanced methanol selectivity over the catalyst with a large particle size stems from the suppression of RWGS reaction. In comparison, Van den Berg et al. [131] have studied the size effect of Cu particles supported on different carriers with the particle size ranging from 2 to 15 nm and concluded that the catalytic activity for CO_2 hydrogenation to methanol is close correlated with the particle size for each group of the catalysts. Smaller particles show even worse activity because the reaction takes place only at Cu sites with a special configuration, e.g., step edge sites, which are not favorable on smaller particles [131]. This work again demonstrated the impact of the microenvironment that superimposes the size effect.

Although the size of metal particles can be tuned by changing the loading of metal content by wet impregnation [246,247] or choosing a porous host with suitable pore size [248], the possible morphological evolution under reaction conditions (e.g., with high pressure, high temperature and the presence of reactants) may lead to even more uncontrollable results [140,142,249]. From this aspect, the MOF template could be a choice to stabilize the metal particles [123,189].

3.5. Oxygen Vacancies

The less coordination of the atoms at defect sites often makes them more reactive than bulk or facet atoms [250–252]. The role of such sites has been extensively reported, such as the stepped Cu in the formation of Cu-Zn alloy, the oxygen vacancies on ZnO for CO hydrogenation, the in-plane sulfur vacancies for the CO_2 dissociation and hydrogen activation, and oxygen vacancies in In_2O_3 for CO_2 adsorption.

For CO_2 hydrogenation over Cu/ZnO catalysts, although the active site was proposed to be the Cu–ZnO interface, the formation of such interface is always accompanied by the formation of oxygen vacancies. In other words, it seems that the latter triggers the formation of Zn–Cu alloy and then the Cu–ZnO interface. Different from the Cu/ZnO system, for Cu supported on ZrO_2, oxygen vacancies functionalize through activating CO_2 [118,253] (One may note that the statement that the activation of CO_2 is the rate-determining step for CO_2 hydrogenation or enhanced CO_2 adsorption will benefit the hydrogenation activity is restricted to specific catalyst system and cannot be extended to a general case). On pure In_2O_3 catalyst, the oxygen vacancies were thought to activate the CO_2 molecule and stabilize the intermediates [79,83,162]. For the recently reported two-dimensional MoS_2 nanosheet catalysts, the in-plane sulfur vacancies were verified to dissociate CO_2 to CO, which is further hydrogenated to methanol. On Cu/CeO_2 catalyst [117], excess surface oxygen vacancies enhanced the stability of Cu in different oxidation states, which leads to the stabilization of the COOH intermediate at the active sites.

The formation of oxygen vacancies is sensitive to the environment. For instance, the formation energy of oxygen vacancies on Cu/CeO_2(111) ranges from 3.8 to 86.8 kJ/mol depending on the positions, significantly smaller than that on stoichiometric CeO_2(111) surface [254]. The formation is promoted by loading selected metals such as Ni, Ir, Rh, Ru, etc., in In_2O_3 [16,83,161]. The SMSI further stabilizes oxygen vacancies, leading to enhanced activity and stability. Moreover, the formation of oxygen vacancies on In_2O_3 is also facilitated by slightly imperfect lattice mismatching, e.g., supported on monoclinic ZrO_2 [154,162,163].

3.6. Reaction Intermediates and Reaction Pathways

Figure 10 presents the proposed reaction pathways for methanol synthesis over Cu-based catalysts. CO_2 is hydrogenated through two competing pathways via either formate or carboxyl intermediates [255]. CO was considered as starting material as well since methanol can be synthesized via CO intermediate. The dissociation of H_2 was proposed to be the initial stage of the reaction, and then CO_2 reacts with preadsorbed H, where the preadsorbed H indeed enhances the binding energy of CO_2 on Cu and improves the probability for further elemental steps.

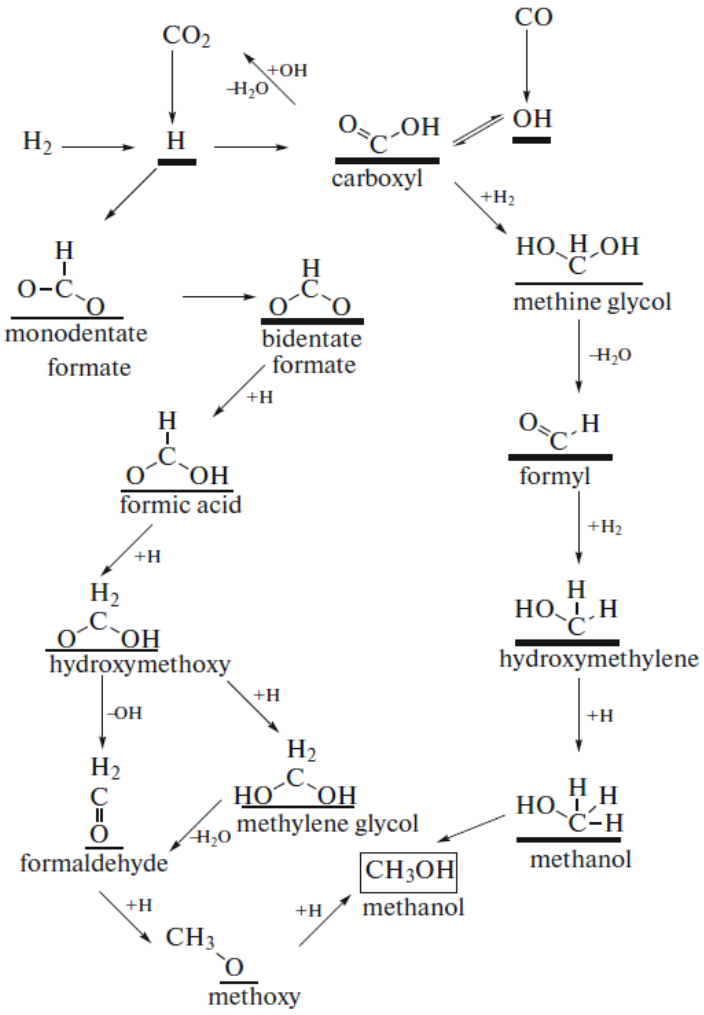


Figure 10. Proposed stepwise mechanism of CO_2 and CO transformations under conditions of methanol synthesis on copper-containing catalysts. Reprinted with permission from ref. [255]. Copyright 2020 Springer.

Varied from the theoretical prediction, Schumacher et al. claimed that carbonate is an important intermediate for CO_2 hydrogenation on Pt(111) surface strained Cu overlayers [256]. They exposed 0.2 bar H_2 to CO_2 pre-exposed Cu/Pt(111) surface and observed a significant loss of surface carbonate species (formed by pre-exposed CO_2). An inference of hydrogenation of carbonate was then drawn based on the experimental findings. The authors explained the missing formate species in the postreaction XPS spectrum by the tensile strain, which lowers the decomposition barrier of formate species and possibly implies structure-sensitive intermediates and reaction pathways.

On Ni/In_2O_3 catalyst, a typical reaction pathway via formate pathway and RWGS pathway is shown in Figure 11 [257]. For both Ni_4/In_2O_3_P and Ni_4/In_2O_3_P surfaces, the RWGS pathway is the preferable route. The introduction of oxygen vacancies significantly reduces the activation barrier. Hydrogen molecules dissociate over Ni species and then spill over to the interfacial sites for further reaction.

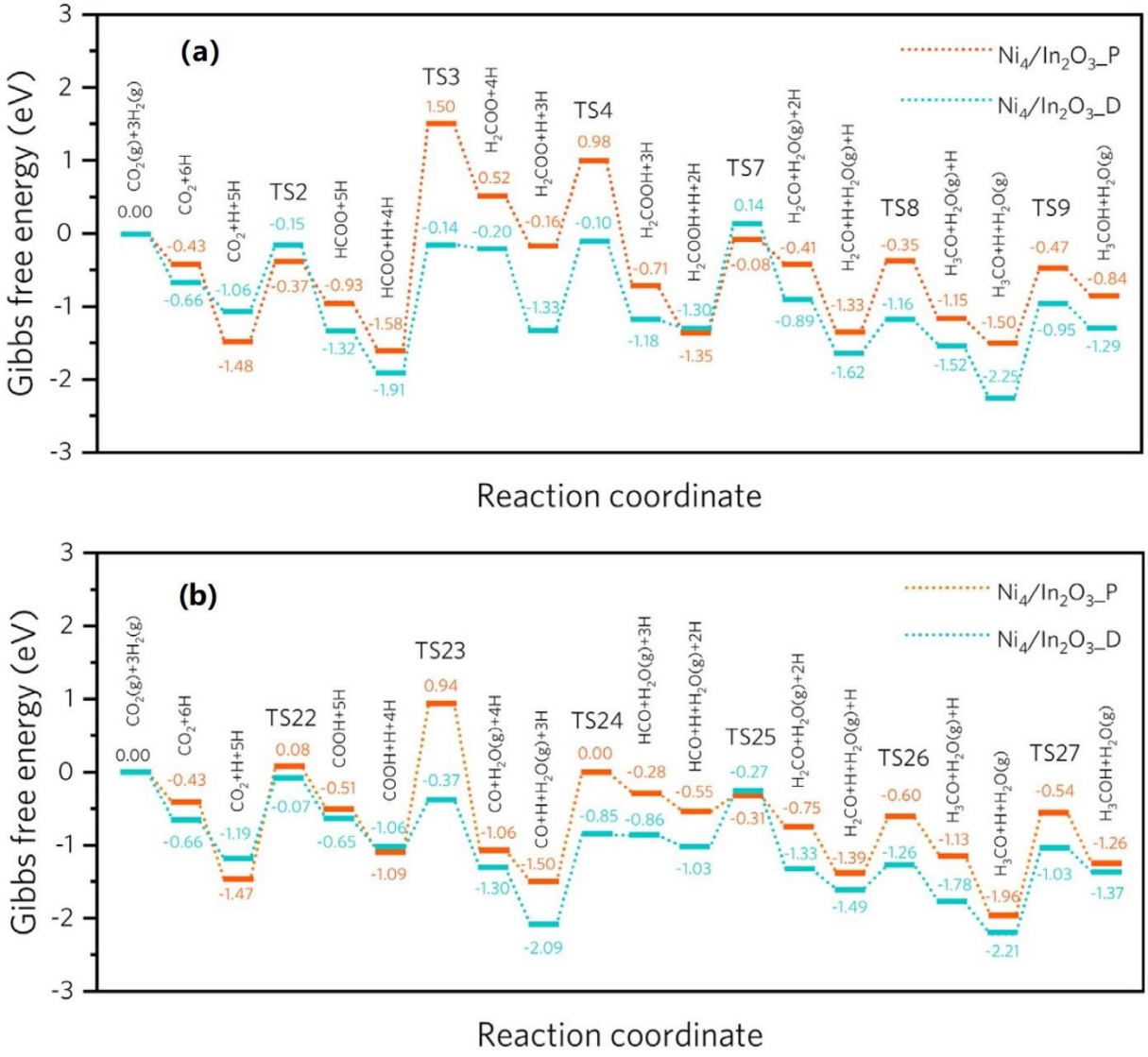


Figure 11. Gibbs energy profiles for CO_2 hydrogenation to methanol over Ni_4/In_2O_3 via the (**a**) formate pathway and (**b**) RWGS pathway. The orange line and blue line represent the Ni_4/In_2O_3_P and Ni_4/In_2O_3_D, respectively. Reprinted with permission from ref. [257]. Copyright 2022 Elsevier.

4. Conclusions and Outlook for Future Work

A catalytic reaction usually consists of a number of essential steps that occur in series. A good catalyst is not necessary to catalyze each of the steps but to uniquely reduce the energy barrier of the rate-determining step or to show the best statistical performance for all steps, which is generally performed by the active site. The rate-determining step, however, is not immutable but correlated with a specific catalyst. This is probably one of the reasons why most of the reported catalysts revolved around a limited number of composites or elements. Microscopic understanding of the structure–activity relationship at the elemental level is worthwhile for the rational development of CO_2 to methanol catalysts. However, one must note that, in most cases, an active site is not a single atomic site with a specific element and chemical state but a series of microscopic locations with distinctive functions and special elemental, electronic and geometric matching for certain specific elemental steps. In other words, catalysis is a multidimensional issue. Therefore, the ultimate aim of the catalyst study is to control the microscopic structure and electronic structure by varying macroscopic parameters (e.g., temperature, pressure, composition, syn-

thesis method, etc.). It seems that we are facing a black box on the way of catalyst development. Catalytic properties are correlated with the composition, geometry, particle size, shape, acid–base properties, chemical states, type of promoters, bonding properties, etc. Particularly, these factors are not isolated but correlative tight or weak, random or regular. This means, especially for the study on the reaction mechanism, the rule drawn on a catalyst through systematically changing certain factors might be misled by the concomitant factors. Conclusions must be drawn with care. In addition, the dynamic structural evolution of catalysts under reaction conditions brings more complexity to the issue (note that the structural evolution is not always negative for activity). At this point, operando techniques would benefit the mechanistic study [258–262]. For the same reason, DFT-derived energy and activation barriers are sensitive to the coverage of surface species. Kinetic analysis may reveal more details about the reaction [263–265]. Besides, machine learning has shown its unique advantages in material science as well as the mechanistic understanding of active sites, which could be a new branch of catalyst development [266–268].

Significant progress has been made on the development of the catalyst for CO_2 hydrogenation to methanol, including improving activity, selectivity, stability, microscopic understanding of the structure-activity relationship, prediction of new catalysts, etc., on the laboratory scale. The reported STY_{CH3OH} and selectivity per se are high enough for the industrial application (e.g., a typical STY of methanol from syngas is roughly estimated to be about 0.5 $g \cdot g_{cat}^{-1} h^{-1}$ [97]). Catalyst development at a larger scale, including synthesis of catalysts, evaluation of activity and stability (e.g., chemical, mechanical, and thermal stability), etc., may fasten the industrialization objective.

Author Contributions: Conceptualization: M.R., X.W., and H.Q.; validation: M.R., X.W., Y.Z., and H.Q.; formal analysis: M.R., X.W., and H.Q.; writing—original draft preparation: M.R., Y.Z., X.W., and H.Q.; writing—review and editing: X.W. and H.Q.; supervision: H.Q.; funding acquisition: H.Q. All authors have read and agreed to the published version of the manuscript.

Funding: This research was funded by National Natural Science Foundation of China, grant number 21972128.

Institutional Review Board Statement: Not applicable.

Informed Consent Statement: Not applicable.

Data Availability Statement: Not applicable.

Acknowledgments: This work was supported by the National Natural Science Foundation of China (Project No. 21972128). We thank Yu Liu for carefully reading the manuscript.

Conflicts of Interest: The authors declare no conflict of interest.

Abbreviation

IR	Infrared
CCS	Carbon Capture and Storage
HOMO	Highest Occupied Molecular Orbital
LUMO	Lowest Unoccupied Molecular Orbital
LPG	Liquefied Petroleum Gas
MTH	Methanol to Hydrocarbons
MTO	Methanol to Olefin
MTA	Methanol to Aromatics
MTG	Methanol to Gasoline
FTS	Fischer-Tropsch Synthesis
RWGS	Reverse Water Gas Shift
DRM	Dry Reforming of Methane
SMSI	Strong Metal–Support Interaction
ICI Ltd.	Imperial Chemical Industries Ltd.
AE	Ammonia Evaporation
FSP	Flame Spray Pyrolysis

MOFs	Metal-Organic Frameworks
GHSV	Gas Hourly Space Velocity
CNTs	Carbon Nanotubes
SOMC	Surface Organometallic Chemistry
NPs	Nanoparticles
DFT	Density Functional Theory
KMC	Kinetic Monte Carlo
ML	Monolayer
UHV	Ultra-High Vacuum
NMR	Nuclear Magnetic Resonance
XPS	X-ray Photoelectron Spectroscopy
HREELS	High-Resolution Electron Energy Loss Spectroscopy
XRD	X-ray Diffraction
XANES	X-ray Absorption Near-Edge Structure
NAP-XPS	Near Ambient Pressure X-ray Photoelectron Spectroscopy
UPS	Ultraviolet Photoelectron Spectroscopy
LEED	Low Energy Electron Diffraction
TEM	Transmission Electron Microscopy
TOF	Turnover Frequency
STY	Space-time Yield
TOS	Time on Stream
CB	Conduction Band
VB	Valence Band

References

1. Freund, H.-J.; Roberts, M. Surface chemistry of carbon dioxide. *Surf. Sci. Rep.* **1996**, *25*, 225–273. https://doi.org/10.1016/s0167-5729(96)00007-6.
2. Leung, D.Y.C.; Caramanna, G.; Maroto-Valer, M.M. An overview of current status of carbon dioxide capture and storage technologies. *Renew. Sustain. Energy Rev.* **2014**, *39*, 426–443. https://doi.org/10.1016/j.rser.2014.07.093.
3. Liu, M.; Yi, Y.; Wang, L.; Guo, H.; Bogaerts, A. Hydrogenation of Carbon Dioxide to Value-Added Chemicals by Heterogeneous Catalysis and Plasma Catalysis. *Catalysts* **2019**, *9*, 275. https://doi.org/10.3390/catal9030275.
4. Keeling, R.F.; Keeling, C.D. Atmospheric Monthly in Situ CO_2 Data-Mauna Loa Observatory, Hawaii (Archive 2021-09-07). In Scripps CO_2 Program Data. UC San Diego Library Digital Collections. Available online: https://library.ucsd.edu/dc/object/bb3859642r (accessed on 1 March 2022).
5. Anderson, T.R.; Hawkins, E.; Jones, P.D. CO_2, the greenhouse effect and global warming: from the pioneering work of Arrhenius and Callendar to today's Earth System Models. *Endeavour* **2016**, *40*, 178–187. https://doi.org/10.1016/j.endeavour.2016.07.002.
6. Wang, W.-H.; Himeda, Y.; Muckerman, J.T.; Manbeck, G.F.; Fujita, E. CO_2 Hydrogenation to Formate and Methanol as an Alternative to Photo- and Electrochemical CO_2 Reduction. *Chem. Rev.* **2015**, *115*, 12936–12973. https://doi.org/10.1021/acs.chemrev.5b00197.
7. Mukherjee, S.; Sikdar, N.; O'nolan, D.; Franz, D.M.; Gascón, V.; Kumar, A.; Kumar, N.; Scott, H.S.; Madden, D.G.; Kruger, P.E.; et al. Trace CO_2 capture by an ultramicroporous physisorbent with low water affinity. *Sci. Adv.* **2019**, *5*, eaax9171. https://doi.org/10.1126/sciadv.aax9171.
8. Service, R.F. ENERGY Carbon capture marches toward practical use *Science* **2021**, *371*, 1300–1300.
9. Yu, K.M.K.; Curcic, I.; Gabriel, J.; Tsang, S.C.E. Recent Advances in CO_2Capture and Utilization. *ChemSusChem* **2008**, *1*, 893–899. https://doi.org/10.1002/cssc.200800169.
10. Kumari, N.; Haider, M.A.; Agarwal, M.; Sinha, N.; Basu, S. Role of Reduced CeO_2(110) Surface for CO_2 Reduction to CO and Methanol. *J. Phys. Chem. C* **2016**, *120*, 16626–16635. https://doi.org/10.1021/acs.jpcc.6b02860.
11. Wang, X.; Maroto-Valer, M.M. Integration of CO_2 Capture and Mineral Carbonation by Using Recyclable Ammonium Salts. *ChemSusChem* **2011**, *4*, 1291–1300. https://doi.org/10.1002/cssc.201000441.
12. Wang, X.L.; Maroto-Valer, M.; Integration of CO_2 capture and storage based on pH-swing mineral carbonation using recyclable ammonium salts. In Proceedings of the 10th International Conference on Greenhouse Gas Control TechnologiesAmsterdam, Amsterdam, The Netherlands, 19–23 September 2010; pp. 4930-4936.
13. Lee, J.W.; Li, R. Integration of fossil energy systems with CO_2 sequestration through NH4HCO3 production. *Energy Convers. Manag.* **2003**, *44*, 1535–1546. https://doi.org/10.1016/s0196-8904(02)00149-8.
14. Bakhtiary-Davijany, H.; Hayer, F.; Phan, X.K.; Myrstad, R.; Venvik, H.J.; Pfeifer, P.; Holmen, A. Characteristics of an Integrated Micro Packed Bed Reactor-Heat Exchanger for methanol synthesis from syngas. *Chem. Eng. J.* **2011**, *167*, 496–503. https://doi.org/10.1016/j.cej.2010.08.074.

15. Duyar, M.S.; Gallo, A.; Regli, S.K.; Snider, J.L.; Singh, J.A.; Valle, E.; McEnaney, J.; Bent, S.F.; Rønning, M.; Jaramillo, T.F. Understanding Selectivity in CO_2 Hydrogenation to Methanol for MoP Nanoparticle Catalysts Using In Situ Techniques. *Catalysts* **2021**, *11*, 143. https://doi.org/10.3390/catal11010143.
16. Wang, J.; Sun, K.; Jia, X.; Liu, C.-J. CO_2 hydrogenation to methanol over Rh/In2O3 catalyst. *Catal. Today* **2021**, *365*, 341–347. https://doi.org/10.1016/j.cattod.2020.05.020.
17. Baraj, E.; Vagaský, S.; Hlinčik, T.; Ciahotný, K.; Tekáč, V. Reaction mechanisms of carbon dioxide methanation. *Chem. Pap.* **2016**, *70*. https://doi.org/10.1515/chempap-2015-0216.
18. Le, T.A.; Kim, J.; Kang, J.K.; Park, E.D. CO and CO_2 methanation over M (M Mn, Ce, Zr, Mg, K, Zn, or V)-promoted Ni/Al@Al2O3 catalysts. *Catal. Today* **2020**, *348*, 80–88. https://doi.org/10.1016/j.cattod.2019.08.058.
19. Le, T.A.; Kim, M.S.; Lee, S.H.; Kim, T.W.; Park, E.D. CO and CO_2 methanation over supported Ni catalysts. *Catal. Today* **2017**, *293-294*, 89–96. https://doi.org/10.1016/j.cattod.2016.12.036.
20. Zheng, Y.; Xu, C.; Zhang, X.; Wu, Q.; Liu, J. Synergistic Effect of Alkali Na and K Promoter on Fe-Co-Cu-Al Catalysts for CO_2 Hydrogenation to Light Hydrocarbons. *Catalysts* **2021**, *11*, 735. https://doi.org/10.3390/catal11060735.
21. Jiang, F.; Liu, B.; Geng, S.; Xu, Y.; Liu, X. Hydrogenation of CO_2 into hydrocarbons: enhanced catalytic activity over Fe-based Fischer–Tropsch catalysts. *Catal. Sci. Technol.* **2018**, *8*, 4097–4107. https://doi.org/10.1039/c8cy00850g.
22. Rodemerck, U.; Holeňa, M.; Wagner, I.E.; Smejkal, Q.; Barkschat, A.; Baerns, E.D.M. Catalyst Development for CO_2 Hydrogenation to Fuels. *ChemCatChem* **2013**, *5*, 1948–1955. https://doi.org/10.1002/cctc.201200879.
23. Eid, K.; Lu, Q.; Abdel-Azeim, S.; Soliman, A.; Abdullah, A.M.; Abdelgwad, A.M.; Forbes, R.P.; Ozoemena, K.I.; Varma, R.S.; Shibl, M.F. Highly exfoliated Ti3C2Tx MXene nanosheets atomically doped with Cu for efficient electrochemical CO_2 reduction: an experimental and theoretical study. *J. Mater. Chem. A* **2021**, *10*, 1965–1975. https://doi.org/10.1039/d1ta09471h.
24. Lu, Q.; Eid, K.; Li, W.; Abdullah, A.M.; Xu, G.; Varma, R.S. Engineering graphitic carbon nitride (g-C3N4) for catalytic reduction of CO_2 to fuels and chemicals: strategy and mechanism. *Green Chem.* **2021**, *23*, 5394–5428. https://doi.org/10.1039/d1gc01303c.
25. Turner, J.; Sverdrup, G.; Mann, M.K.; Maness, P.C.; Kroposki, B.; Ghirardi, M.; Evans, R.J.; Blake, D. Renewable hydrogen production. *Int. J. Energy Res.* **2008**, 32, 379–407. https://doi.org/10.1002/er.1372.
26. Mondal, B.; Song, J.; Neese, F.; Ye, S. Bio-inspired mechanistic insights into CO_2 reduction. *Curr. Opin. Chem. Biol.* **2015**, *25*, 103–109. https://doi.org/10.1016/j.cbpa.2014.12.022.
27. Cooper, C.; Compton, R. Metastable anions of CO_2. *Chem. Phys. Lett.* **1972**, *14*, 29–32. https://doi.org/10.1016/0009-2614(72)87133-1.
28. Álvarez, A.; Borges, M.; Corral-Pérez, J.J.; Olcina, J.G.; Hu, L.; Cornu, D.; Huang, R.; Stoian, D.; Urakawa, A. CO_2Activation over Catalytic Surfaces. *ChemPhysChem* **2017**, *18*, 3135–3141. https://doi.org/10.1002/cphc.201700782.
29. Yang, T.; Gu, T.; Han, Y.; Wang, W.; Yu, Y.; Zang, Y.; Zhang, H.; Mao, B.; Li, Y.; Yang, B.; et al. Surface Orientation and Pressure Dependence of CO_2 Activation on Cu Surfaces. *J. Phys. Chem. C* **2020**, *124*, 27511–27518. https://doi.org/10.1021/acs.jpcc.0c08262.
30. Eren, B.; Weatherup, R.S.; Liakakos, N.; Somorjai, G.A.; Salmeron, M. Dissociative Carbon Dioxide Adsorption and Morphological Changes on Cu(100) and Cu(111) at Ambient Pressures. *J. Am. Chem. Soc.* **2016**, *138*, 8207–8211. https://doi.org/10.1021/jacs.6b04039.
31. Fu, S.S.; Somorjai, G.A. Interactions of O_2, CO, CO_2, and D2 with the stepped Cu(311) crystal face: Comparison to Cu(110). *Surf. Sci.* **1992**, *262*, 68–76. https://doi.org/10.1016/0039-6028(92)90460-N.
32. Hagman, B.; Posada-Borbón, A.; Schaefer, A.; Shipilin, M.; Zhang, C.; Merte, L.R.; Hellman, A.; Lundgren, E.; Grönbeck, H.; Gustafson, J. Steps Control the Dissociation of CO_2 on Cu(100). *J. Am. Chem. Soc.* **2018**, *140*, 12974–12979. https://doi.org/10.1021/jacs.8b07906.
33. Onsgaard, J.; Thomsen, L.; Hoffmann, S.V.; Godowski, P.J. Surface reactions between CO_2 and H over K-modified Cu(001). *Vac.* **2006**, *81*, 25–31. https://doi.org/10.1016/j.vacuum.2006.02.005.
34. Ahmad, W.; Al-Matar, A.; Shawabkeh, R.; Rana, A. An experimental and thermodynamic study for conversion of CO_2 to CO and methane over Cu-K/Al2O3. *J. Environ. Chem. Eng.* **2016**, *4*, 2725–2735. https://doi.org/10.1016/j.jece.2016.05.019.
35. Koitaya, T.; Yamamoto, S.; Shiozawa, Y.; Yoshikura, Y.; Hasegawa, M.; Tang, J.; Takeuchi, K.; Mukai, K.; Yoshimoto, S.; Matsuda, I.; et al. CO_2 Activation and Reaction on Zn-Deposited Cu Surfaces Studied by Ambient-Pressure X-ray Photoelectron Spectroscopy. *ACS Catal.* **2019**, *9*, 4539–4550. https://doi.org/10.1021/acscatal.9b00041.
36. Vesselli, E.; De Rogatis, L.; Ding, X.; Baraldi, A.; Savio, L.; Vattuone, L.; Rocca, M.; Fornasiero, P.; Peressi, M.; Baldereschi, A.; et al. Carbon Dioxide Hydrogenation on Ni(110). *J. Am. Chem. Soc.* **2008**, *130*, 11417–11422. https://doi.org/10.1021/ja802554g.
37. Wang, Y.; Kováčik, R.; Meyer, B.; Kotsis, K.; Stodt, D.; Staemmler, V.; Qiu, H.; Traeger, F.; Langenberg, D.; Muhler, M.; et al. CO_2 Activation by ZnO through the Formation of an Unusual Tridentate Surface Carbonate. *Angew. Chem. Int. Ed.* **2007**, *46*, 5624–5627. https://doi.org/10.1002/anie.200700564.
38. Wang, Y.; Xia, X.; Urban, A.; Qiu, H.; Strunk, J.; Meyer, B.; Muhler, M.; Wöll, C. Tuning the Reactivity of Oxide Surfaces by Charge-Accepting Adsorbates. *Angew. Chem. Int. Ed.* **2007**, *46*, 7315–7318. https://doi.org/10.1002/anie.200702815.
39. Wang, Y.; Lafosse, A.; Jacobi, K. Adsorption and Reaction of CO_2 on the RuO2(110) Surface. *J. Phys. Chem. B* **2002**, *106*, 5476–5482. https://doi.org/10.1021/jp025619x.
40. Kossmann, J.; Rossmuller, G.; Hattig, C. Prediction of vibrational frequencies of possible intermediates and side products of the methanol synthesis on ZnO(000(1)over-bar) by ab initio calculations. *J. Chem. Phys.***2012**, 136,034706. https://doi.org/10.1063/1.3671450.

41. Bligaard, T.; Norskov, J.K.; Dahl, S.; Matthiesen, J.; Christensen, C.H.; Sehested, J. The Bronsted-Evans-Polanyi relation and the volcano curve in heterogeneous catalysis. *J. Catal.* **2004**, 224, 206–217. https://doi.org/10.1016/j.jcat.2004.02.034.
42. Ye, J.; Liu, C.; Mei, D.; Ge, Q. Active Oxygen Vacancy Site for Methanol Synthesis from CO_2 Hydrogenation on In2O3(110): A DFT Study. *ACS Catal.* **2013**, *3*, 1296–1306. https://doi.org/10.1021/cs400132a.
43. Li, S.; Guo, L.; Ishihara, T. Hydrogenation of CO_2 to methanol over Cu/AlCeO catalyst. *Catal. Today* **2020**, *339*, 352–361. https://doi.org/10.1016/j.cattod.2019.01.015.
44. Olah, G.A. Beyond Oil and Gas: The Methanol Economy. *Angew. Chem. Int. Ed.* **2005**, *44*, 2636–2639. https://doi.org/10.1002/anie.200462121.
45. Joo, O.-S.; Jung, K.-D.; Moon, I.; Rozovskii, A.Y.; Lin, G.I.; Han, S.-H.; Uhm, S.-J. Carbon Dioxide Hydrogenation to Form Methanol via a Reverse-Water-Gas-Shift Reaction (the CAMERE Process). *Ind. Eng. Chem. Res.* **1999**, *38*, 1808–1812. https://doi.org/10.1021/ie9806848.
46. Bermúdez, J.; Fidalgo, B.; Arenillas, A.; Menéndez, J. Dry reforming of coke oven gases over activated carbon to produce syngas for methanol synthesis. *Fuel* **2010**, *89*, 2897–2902. https://doi.org/10.1016/j.fuel.2010.01.014.
47. Al-Dossary, M.; Ismail, A.A.; Fierro, J.; Bouzid, H.; Al-Sayari, S. Effect of Mn loading onto MnFeO nanocomposites for the CO_2 hydrogenation reaction. *Appl. Catal. B: Environ.* **2015**, *165*, 651–660. https://doi.org/10.1016/j.apcatb.2014.10.064.
48. Tang, M.; Xu, L.; Fan, M. Effect of Ce on 5 wt% Ni/ZSM-5 catalysts in the CO_2 reforming of CH4 reaction. *Int. J. Hydrogen Energy* **2014**, *39*, 15482–15496. https://doi.org/10.1016/j.ijhydene.2014.07.172.
49. Tahir, B.; Tahir, M.; Amin, N.A.S. Ag-La loaded protonated carbon nitrides nanotubes (pCNNT) with improved charge separation in a monolithic honeycomb photoreactor for enhanced bireforming of methane (BRM) to fuels. *Appl. Catal. B: Environ.* **2019**, *248*, 167–183. https://doi.org/10.1016/j.apcatb.2019.01.076.
50. Chiang, C.-L.; Lin, K.-S.; Chuang, H.-W. Direct synthesis of formic acid via CO_2 hydrogenation over Cu/ZnO/Al2O3 catalyst. *J. Clean. Prod.* **2018**, *172*, 1957–1977. https://doi.org/10.1016/j.jclepro.2017.11.229.
51. Yadav, V.S.K.; Purkait, M.K. Synthesis of Pb2O electrocatalyst and its application in the electrochemical reduction of CO_2 to HCOOH in various electrolytes. *RSC Adv.* **2015**, *5*, 40414–40421. https://doi.org/10.1039/c5ra05899f.
52. Zhou, X.; Su, T.; Jiang, Y.Z.; Qin, H.; Ji, Z. Guo, CuO-Fe_2O_3-CeO_2/HZSM-5 bifunctional catalyst hydrogenated CO_2 for enhanced dimethyl ether synthesis. *Chem. Eng. Sci.* **2016**, *153*, 10–20. https://doi.org/10.1016/j.ces.2016.07.007.
53. Dubois, J.-L.; Sayama, K.; Arakawa, H. Conversion of CO_2 to dimethylether and methanol over hybrid catalysts. *Chem. Lett.* 1992, *21*, 1115–1118. https://doi.org/10.1246/cl.1992.1115.
54. Mohammadkhani, B.; Haghighi, M.; Sadeghpour, P. Altering C2H4/C3H6 yield in methanol to light olefins over HZSM-5, SAPO-34 and SAPO-34/HZSM-5 nanostructured catalysts: influence of Si/Al ratio and composite formation. *RSC Advances* **2016**, 6, 25460–25471. https://doi.org/10.1039/C6RA00432F.
55. Charghand, M.; Haghighi, M.; Saedy, S.; Aghamohammadi, S. Efficient hydrothermal synthesis of nanostructured SAPO-34 using ultrasound energy: Physicochemical characterization and catalytic performance toward methanol conversion to light olefins. *Adv. Powder Technol.* **2014**, *25*, 1728–1736. https://doi.org/10.1016/j.apt.2014.06.022.
56. Cui, X.; Kær, S.K. A comparative study on three reactor types for methanol synthesis from syngas and CO_2. *Chem. Eng. J.* **2020**, *393*, 124632. https://doi.org/10.1016/j.cej.2020.124632.
57. Li, S.; Krishnamoorthy, S.; Li, A.; Meitzner, G.D.; Iglesia, E. Promoted Iron-Based Catalysts for the Fischer–Tropsch Synthesis: Design, Synthesis, Site Densities, and Catalytic Properties. *J. Catal.* **2002**, *206*, 202–217. https://doi.org/10.1006/jcat.2001.3506.
58. Ghogia, A.C.; Nzihou, A.; Serp, P.; Soulantica, K.; Minh, D.P. Cobalt catalysts on carbon-based materials for Fischer-Tropsch synthesis: a review. *Appl. Catal. A: Gen.* **2020**, *609*, 117906. https://doi.org/10.1016/j.apcata.2020.117906.
59. Chen, Y.; Wei, J.; Duyar, M.S.; Ordomsky, V.V.; Khodakov, A.Y.; Liu, J. Carbon-based catalysts for Fischer–Tropsch synthesis. *Chem. Soc. Rev.* **2021**, *50*, 2337–2366. https://doi.org/10.1039/d0cs00905a.
60. Ortega, C.; Hessel, V.; Kolb, G. Dimethyl ether to hydrocarbons over ZSM-5: Kinetic study in an external recycle reactor. *Chem. Eng. J.* **2018**, *354*, 21–34. https://doi.org/10.1016/j.cej.2018.07.178.
61. Behrens, M. Promoting the Synthesis of Methanol: Understanding the Requirements for an Industrial Catalyst for the Conversion of CO_2. *Angew. Chem. Int. Ed.* **2016**, *55*, 14906–14908. https://doi.org/10.1002/anie.201607600.
62. Gao, P.; Zhong, L.; Zhang, L.; Wang, H.; Zhao, N.; Wei, W.; Sun, Y. Yttrium oxide modified Cu/ZnO/Al2O3catalysts via hydrotalcite-like precursors for CO_2hydrogenation to methanol. *Catal. Sci. Technol.* **2015**, *5*, 4365–4377. https://doi.org/10.1039/c5cy00372e.
63. Toyir, J.; de la Piscina, P.R.; Fierro, J.L.G.; Homs, N. Highly effective conversion of CO_2 to methanol over supported and promoted copper-based catalysts: influence of support and promoter. *Appl. Catal. B: Environ.* **2001**, *29*, 207–215. https://doi.org/10.1016/s0926-3373(00)00205-8.
64. Yang, H.; Zhang, C.; Gao, P.; Wang, H.; Li, X.; Zhong, L.; Wei, W.; Sun, Y. A review of the catalytic hydrogenation of carbon dioxide into value-added hydrocarbons. *Catal. Sci. Technol.* **2017**, *7*, 4580–4598. https://doi.org/10.1039/c7cy01403a.
65. Wang, Y.H.; Gao, W.G.; Li, K.Z.; Zheng, Y.N.; Xie, Z.H.; Na, W.; Chen, J.G.; Wang, H. Strong Evidence of the Role of H_2O in Affecting Methanol Selectivity from CO_2 Hydrogenation over Cu-ZnO-ZrO2. *Chem* **2020**, *6*, 419–430.
66. Wang, W.; Tongo, D.W.K.; Song, L.; Qu, Z. Effect of Au Addition on the Catalytic Performance of CuO/CeO2 Catalysts for CO_2 Hydrogenation to Methanol. *Top. Catal.* **2021**, *64*, 446–455. https://doi.org/10.1007/s11244-021-01414-3.
67. Salehi, M.-S.; Askarishahi, M.; Gallucci, F.; Godini, H.R. Selective CO_2-Hydrogenation using a membrane reactor. *Chem. Eng. Process. Process Intensif.* **2021**, *160*, 108264. https://doi.org/10.1016/j.cep.2020.108264.

68. Zhu, J.; Su, Y.-Q.; Chai, J.; Muravev, V.; Kosinov, N.; Hensen, E. Mechanism and Nature of Active Sites for Methanol Synthesis from CO/CO_2 on Cu/CeO_2. *ACS Catal.* **2020**, *10*, 11532–11544. https://doi.org/10.1021/acscatal.0c02909.
69. Oshima, K.; Honma, Y.; Kinoshita, K.; Gao, Z.; Honma, T.; Tada, S.; Satokawa, S. Mechanochemical Effect in Mixing Sponge Copper with Amorphous ZrO2 Creates Effective Active Sites for Methanol Synthesis by CO_2 Hydrogenation. *J. Phys. Chem. C* **2021**, *125*, 8155–8162. https://doi.org/10.1021/acs.jpcc.0c10917.
70. Chen, S.; Zhang, J.; Song, F.; Zhang, Q.; Yang, G.; Zhang, M.; Wang, X.; Xie, H.; Tan, Y. Induced high selectivity methanol formation during CO_2 hydrogenation over a CuBr2-modified CuZnZr catalyst. *J. Catal.* **2020**, *389*, 47–59. https://doi.org/10.1016/j.jcat.2020.05.023.
71. Xu, D.; Hong, X.; Liu, G. Highly dispersed metal doping to ZnZr oxide catalyst for CO_2 hydrogenation to methanol: Insight into hydrogen spillover. *J. Catal.* **2021**, *393*, 207–214. https://doi.org/10.1016/j.jcat.2020.11.039.
72. Li, M.M.J.; Zou, H.B.; Zheng, J.W.;Wu, T.S.; Chan, T.S.; Soo, Y.L.; Wu, X.P.; Gong, X.Q.; Chen, T.Y.; Roy, K.; Held, G.; Tsang, S.C.E. Methanol Synthesis at a Wide Range of H-2/CO(2)Ratios over a Rh-In Bimetallic Catalyst *Angew. Chem.-Int. Edit.* **2020**, *59*, 16039–16046.
73. Mureddu, M.; Lai, S.; Atzori, L.; Rombi, E.; Ferrara, F.; Pettinau, A.; Cutrufello, M. Ex-LDH-Based Catalysts for CO_2 Conversion to Methanol and Dimethyl Ether. *Catalysts* **2021**, *11*, 615. https://doi.org/10.3390/catal11050615.
74. Han, Z.; Tang, C.Z.; Sha, F.; Tang, S.; Wang, J.J.; Li, C. CO_2 hydrogenation to methanol on ZnO-ZrO2 solid solution catalysts with ordered mesoporous structure *J. Catal.* **2021**, *396*, 242–250.
75. Wu, C.Y.; Lin, L.L.; Liu, J.J.; Zhang, J.P.; Zhang, F.; Zhou, T.; Rui, N.; Yao, S.Y.; Deng, Y.C.; Yang, F.; et al. Inverse ZrO2/Cu as a highly efficient methanol synthesis catalyst from CO_2 hydrogenation. *Nat. Commun.* **2020**, doi:1038/s41467-020-19634-8
76. Wang, W.; Qu, Z.; Song, L.; Fu, Q. Effect of the nature of copper species on methanol synthesis from CO_2 hydrogenation reaction over CuO/Ce0.4Zr0.6O2 catalyst. *Mol. Catal.* **2020**, *493*, 111105. https://doi.org/10.1016/j.mcat.2020.111105.
77. Ghosh, S.; Sebastian, J.; Olsson, L.; Creaser, D. Experimental and kinetic modeling studies of methanol synthesis from CO_2 hydrogenation using In2O3 catalyst. *Chem. Eng. J.* **2021**, *416*, 129120. https://doi.org/10.1016/j.cej.2021.129120.
78. Pustovarenko, A.; Dikhtiarenko, A.; Bavykina, A.; Gevers, L.E.; Ramírez, A.; Russkikh, A.; Telalovic, S.; Aguilar, A.; Hazemann, J.-L.; Ould-Chikh, S.; et al. Metal–Organic Framework-Derived Synthesis of Cobalt Indium Catalysts for the Hydrogenation of CO_2 to Methanol. *ACS Catal.* **2020**, *10*, 5064–5076. https://doi.org/10.1021/acscatal.0c00449.
79. Martin, O.; Martín, A.J.; Mondelli, C.; Mitchell, S.; Segawa, T.F.; Hauert, R.; Drouilly, C.; Curulla-Ferré, D.; Pérez-Ramírez, J. Indium Oxide as a Superior Catalyst for Methanol Synthesis by CO_2 Hydrogenation. *Angew. Chem. Int. Ed.* **2016**, *55*, 6261–6265. https://doi.org/10.1002/anie.201600943.
80. Rui, N.; Zhang, F.; Sun, K.H.; Liu, Z.Y.; Xu, W.Q.; Stavitski, E.; Senanayake, S.D.; Rodriguez, J.A.; Liu, C.J. Hydrogenation of CO_2 to Methanol on a Au delta+-In2O3-x Catalyst. *ACS Catal.* **2020**, *10*, 11307–11317. https://doi.org/10.1021/acscatal.0c02120.
81. Yao, L.; Pan, Y.; Wu, D.; Li, J.; Xie, R.; Peng, Z. Approaching full-range selectivity control in CO_2 hydrogenation to methanol and carbon monoxide with catalyst composition regulation. *Inorg. Chem. Front.* **2021**, *8*, 2433–2441. https://doi.org/10.1039/d1qi00129a.
82. Fang, T.; Liu, B.; Lian, Y.; Zhang, Z. Selective Methanol Synthesis from CO_2 Hydrogenation over an In2O3/Co/C-N Catalyst. *Ind. Eng. Chem. Res.* **2020**, *59*, 19162–19167. https://doi.org/10.1021/acs.iecr.0c02639.
83. Shen, C.Y.; Sun, K.H.; Zhang, Z.T.; Rui, N.; Jia, X.Y.; Mei, D.H.; Liu, C.J. Highly Active Ir/In2O3 Catalysts for Selective Hydrogenation of CO_2 to Methanol: Experimental and Theoretical Studies. *ACS Catal.* **2021**, *11*, 4036–4046. https://doi.org/10.1021/acscatal.0c05628.
84. 80. Z. Lu, K.H. Sun, J. Wang, Z.T. Zhang, C.J. Liu, A Highly Active Au/In2O3-ZrO2 Catalyst for Selective Hydrogenation of CO_2 to Methanol. *Catalysts* **2020**, *10*, 1360. https://doi.org/10.3390/catal10111360.
85. Feng, W.-H.; Yu, M.-M.; Wang, L.-J.; Miao, Y.-T.; Shakouri, M.; Ran, J.; Hu, Y.; Li, Z.; Huang, R.; Lu, Y.-L.; et al. Insights into Bimetallic Oxide Synergy during Carbon Dioxide Hydrogenation to Methanol and Dimethyl Ether over GaZrOx Oxide Catalysts. *ACS Catal.* **2021**, *11*, 4704–4711. https://doi.org/10.1021/acscatal.0c05410.
86. Bibi, M.; Ullah, R.; Sadiq, M.; Sadiq, S.; Khan, I.; Saeed, K.; Zia, M.; Iqbal, Z.; Ullah, I.; Iqbal, Z.; et al. Catalytic Hydrogenation of Carbon Dioxide over Magnetic Nanoparticles: Modification in Fixed-Bed Reactor. *Catalysts* **2021**, *11*, 592. https://doi.org/10.3390/catal11050592.
87. Pasupulety, N.; Al-Zahrani, A.A.; Daous, M.A.; Podila, S.; Driss, H. A study on highly active Cu-Zn-Al-K catalyst for CO_2 hydrogenation to methanol. *Arab. J. Chem.* **2020**, *14*, 102951. https://doi.org/10.1016/j.arabjc.2020.102951.
88. Shi, Z.; Tan, Q.; Tian, C.; Pan, Y.; Sun, X.; Zhang, J.; Wu, D. CO_2 hydrogenation to methanol over Cu-In intermetallic catalysts: Effect of reduction temperature. *J. Catal.* **2019**, *379*, 78–89. https://doi.org/10.1016/j.jcat.2019.09.024.
89. Ahmad, K.; Upadhyayula, S. Kinetics of CO_2 hydrogenation to methanol over silica supported intermetallic Ga3Ni5 catalyst in a continuous differential fixed bed reactor. *Int. J. Hydrogen Energy* **2020**, *45*, 1140–1150. https://doi.org/10.1016/j.ijhydene.2019.10.156.
90. Hu, J.; Yu, L.; Deng, J.; Wang, Y.; Cheng, K.; Ma, C.; Zhang, Q.; Wen, W.; Yu, S.; Pan, Y.; et al. Sulfur vacancy-rich MoS2 as a catalyst for the hydrogenation of CO_2 to methanol. *Nat. Catal.* **2021**, *4*, 242–250. https://doi.org/10.1038/s41929-021-00584-3.
91. Gothe, M.; Pérez-Sanz, F.J.; Braga, A.; Borges, L.R.; Abreu, T.F.; Bazito, R.C.; Gonçalves, R.V.; Rossi, L.M.; Vidinha, P. Selective CO_2 hydrogenation into methanol in a supercritical flow process. *J. CO_2 Util.* **2020**, *40*, 101195. https://doi.org/10.1016/j.jcou.2020.101195.

92. Kuwahara, Y.; Mihogi, T.; Hamahara, K.; Kusu, K.; Kobayashi, H.; Yamashita, H. A quasi-stable molybdenum sub-oxide with abundant oxygen vacancies that promotes CO_2 hydrogenation to methanol. *Chem. Sci.* **2021**, *12*, 9902–9915. https://doi.org/10.1039/d1sc02550c.
93. Zabilskiy, M.; Sushkevich, V.L.; Newton, M.A.; Krumeich, F.; Nachtegaal, M.; van Bokhoven, J.A. Mechanistic Study of Carbon Dioxide Hydrogenation over Pd/ZnO-Based Catalysts: The Role of Palladium-Zinc Alloy in Selective Methanol Synthesis. *Angew. Chem.-Int. Edit.* **2021**, *60*, 17053–17059. https://doi.org/10.1002/anie.202103087.
94. Temvuttirojn, C.; Poo-Arporn, Y.; Chanlek, N.; Cheng, C.K.; Chong, C.C.; Limtrakul, J.; Witoon, T. Role of Calcination Temperatures of ZrO2 Support on Methanol Synthesis from CO_2 Hydrogenation at High Reaction Temperatures over ZnOx/ZrO2 Catalysts. *Ind. Eng. Chem. Res.* **2020**, *59*, 5525–5535. https://doi.org/10.1021/acs.iecr.9b05691.
95. Wang, Y.; Wu, D.; Liu, T.; Liu, G.; Hong, X. Fabrication of PdZn alloy catalysts supported on ZnFe composite oxide for CO_2 hydrogenation to methanol. *J. Colloid Interface Sci.* **2021**, *597*, 260–268. https://doi.org/10.1016/j.jcis.2021.03.135.
96. Chinchen, G.C.; Denny, P.J.; Jennings, J.R.; Spencer, M.S.; Waugh, K.C. Synthesis of Methanol .1. Catalysts And Kinetics. *Appl. Catal.* **1998**, *36*, 1–65. https://doi.org/10.1016/S0166-9834(00)80103-7.
97. Klier, K. Methanol Synthesis. *Adv. Catal.* **1982**, *31*, 243–313. https://doi.org/10.1016/S0360-0564(08)60455-1.
98. Behrens, M.; Studt, F.; Kasatkin, I.; Kühl, S.; Hävecker, M.; Abild-Pedersen, F.; Zander, S.; Girgsdies, F.; Kurr, P.; Kniep, B.-L.; et al. The Active Site of Methanol Synthesis over Cu/ZnO/Al 2 O 3 Industrial Catalysts. *Science* **2012**, *336*, 893–897. https://doi.org/10.1126/science.1219831.
99. Chinchen, G.; Denny, P.; Parker, D.; Spencer, M.; Whan, D. Mechanism of methanol synthesis from CO_2/CO/H2 mixtures over copper/zinc oxide/alumina catalysts: use of14C-labelled reactants. *Appl. Catal.* **1987**, *30*, 333–338. https://doi.org/10.1016/s0166-9834(00)84123-8.
100. Liu, G.; Willcox, D.; Garland, M.; Kung, H.H. The Role of CO_2 In Methanol Synthesis on Cu-Zn Oxide: An Isotope Labeling Study, *J. Catal.* **1985**, 96, 251–260. https://doi.org/10.1016/0021-9517(85)90378-1.
101. Zhang, L.X.; Zhang, Y.C.; Chen, S.Y. Effect of promoter SiO2, TiO2 or SiO2-TiO2 on the performance of CuO-ZnO-Al2O3 catalyst for methanol synthesis from CO_2 hydrogenation. *Appl. Catal. Gen.* **2012**, 415, 118–123. https://doi.org/10.1016/j.apcata.2011.12.013.
102. Baltes, C.; Vukojevic, S.; Schuth, F. Correlations between synthesis, precursor, and catalyst structure and activity of a large set of CuO/ZnO/Al2O3 catalysts for methanol synthesis. *J. Catal.* **2008**, *258*, 334–344. https://doi.org/10.1016/j.jcat.2008.07.004.
103. Kattel, S.; Ramírez, P.J.; Chen, J.G.; Rodriguez, J.A.; Liu, P. Active sites for CO_2 hydrogenation to methanol on Cu/ZnO catalysts. *Science* **2017**, *355*, 1296–1299. https://doi.org/10.1126/science.aal3573.
104. Kattel, S.; Ramirez, P.J.; Chen, J.G.G.; Rodriguez, J.A.; Liu, P. Response to Comment on "Active sites for CO_2 hydrogenation to methanol on Cu/ZnO catalysts". *Science* **2017**, 357, 2. https://doi.org/10.1126/science.aan8210.
105. Nakamura, J.; Fujitani, T.; Kuld, S.; Helveg, S.; Chorkendorff, I.; Sehested, J. Comment on "Active sites for CO_2 hydrogenation to methanol on Cu/ZnO catalysts. *Science* **2017**, 357, 2. https://doi.org/10.1126/science.aan8074.
106. Kuld, S.; Thorhauge, M.; Falsig, H.; Elkjaer, C.F.; Helveg, S.; Chorkendorff, I.; Sehested, J. Quantifying the promotion of Cu catalysts by ZnO for methanol synthesis. *Science* **2016**, *352*, 969–974. https://doi.org/10.1126/science.aaf0718.
107. Posada-Perez, S.; Ramirez, P.J.; Gutierrez, R.A.; Stacchiola, D.J.; Vines, F.; Liu, P.; Illas, F.; Rodriguez, J.A. The conversion of CO_2 to methanol on orthorhombic beta-Mo2C and Cu/beta-Mo2C catalysts: mechanism for admetal induced change in the selectivity and activity. *Catal. Sci. Technol.* **2016**, 6, 6766–6777. https://doi.org/10.1039/C5CY02143J.
108. Elnabawy, A.O.; Schimmenti, R.; Cao, A.; Norskov, J.K. Why ZnO is the Support for Cu in Methanol Synthesis? A Systematic Study of the Strong Metal Support Interactions. *ACS Sustain. Chem. Eng.* **2022**, 10, 1722–1730. https://doi.org/10.1021/acssuschemeng.1c07980.
109. Gao, P.; Yang, H.Y.; Zhang, L.N.; Zhang, C.; Zhong, L.S.; Wang, H.; Wei, W.; Sun, Y.H. Fluorinated Cu/Zn/A1/Zr hydrotalcites derived nanocatalysts for CO_2 hydrogenation to methanol. *J. CO_2 Util.* **2016**, 16, 32–41. https://doi.org/10.1016/j.jcou.2016.06.001.
110. Kondrat, S.A.; Smith, P.J.; Wells, P.P.; Chater, P.A.; Carter, J.H.; Morgan, D.J.; Fiordaliso, E.M.; Wagner, J.B.; Davies, T.E.; Lu, L.; et al. Stable amorphous georgeite as a precursor to a high-activity catalyst. *Nature* **2016**, *531*, 83–87. https://doi.org/10.1038/nature16935.
111. Tada, S.; Kayamori, S.; Honma, T.; Kamei, H.; Nariyuki, A.; Kon, K.; Toyao, T.; Shimizu, K.-I.; Satokawa, S. Design of Interfacial Sites between Cu and Amorphous ZrO_2 Dedicated to CO_2-to-Methanol Hydrogenation. *ACS Catal.* **2018**, *8*, 7809–7819. https://doi.org/10.1021/acscatal.8b01396.
112. Yu, J.; Yang, M.; Zhang, J.; Ge, Q.; Zimina, A.; Pruessmann, T.; Zheng, L.; Grunwaldt, J.-D.; Sun, J. Stabilizing Cu+ in Cu/SiO2 Catalysts with a Shattuckite-Like Structure Boosts CO_2 Hydrogenation into Methanol. *ACS Catal.* **2020**, *10*, 14694–14706. https://doi.org/10.1021/acscatal.0c04371.
113. Brown, N.J.; Weiner, J.; Hellgardt, K.; Shaffer, M.S.P.; Williams, C.K. Phosphinate stabilised ZnO and Cu colloidal nanocatalysts for CO_2 hydrogenation to methanol. *Chem. Commun.* **2013**, *49*, 11074–11076. https://doi.org/10.1039/c3cc46203j.
114. Dong, X.; Li, F.; Zhao, N.; Xiao, F.; Wang, J.; Tan, Y. CO_2 hydrogenation to methanol over Cu/ZnO/ZrO2 catalysts prepared by precipitation-reduction method. *Appl. Catal. B: Environ.* **2016**, *191*, 8–17. https://doi.org/10.1016/j.apcatb.2016.03.014.
115. Xiao, S.; Zhang, Y.; Gao, P.; Zhong, L.; Li, X.; Zhang, Z.; Wang, H.; Wei, W.; Sun, Y. Highly efficient Cu-based catalysts via hydrotalcite-like precursors for CO_2 hydrogenation to methanol. *Catal. Today* **2017**, *281*, 327–336. https://doi.org/10.1016/j.cattod.2016.02.004.

116. Conrad, F.; Zhou, Y.; Yulikov, M.; Hametner, K.; Weyeneth, S.; Jeschke, G.; Gunther, D.; Grunwaldt, J.D.; Patzke, G.R. Microwave-Hydrothermal Synthesis of Nanostructured Zinc-Copper Gallates. *Eur. J. Inorg. Chem.* **2010**, 2036–2043. https://doi.org/10.1002/ejic.200901169.
117. Singh, R.; Tripathi, K.; Pant, K.K. Investigating the role of oxygen vacancies and basic site density in tuning methanol selectivity over Cu/CeO2 catalyst during CO_2 hydrogenation. *Fuel* **2021**, *303*, 121289. https://doi.org/10.1016/j.fuel.2021.121289.
118. Sun, Y.H.; Chen, L.M.; Bao, Y.F.; Wang, G.N.; Zhang, Y.J.; Fu, M.L.; Wu, J.L.; Ye, D.Q. Roles of nitrogen species on nitrogen-doped CNTs supported Cu-ZrO2 system for carbon dioxide hydrogenation to methanol. *Catal. Today* **2018** *307*, 212–223. https://doi.org/10.1016/j.cattod.2017.04.017
119. Sharma, S.K.; Paul, B.; Pal, R.S.; Bhanja, P.; Banerjee, A.; Samanta, C.; Bal, R. Influence of Indium as a Promoter on the Stability and Selectivity of the Nanocrystalline Cu/CeO2 Catalyst for CO_2 Hydrogenation to Methanol. *ACS Appl. Mater. Interfaces* **2021**, *13*, 28201–28213. https://doi.org/10.1021/acsami.1c05586.
120. Noh, G.; Lam, E.; Bregante, D.T.; Meyet, J.; Šot, P.; Flaherty, D.W.; Copéret, C. Lewis Acid Strength of Interfacial Metal Sites Drives CH 3 OH Selectivity and Formation Rates on Cu-Based CO_2 Hydrogenation Catalysts. *Angew. Chem. Int. Ed.* **2021**, *60*, 9650–9659. https://doi.org/10.1002/anie.202100672.
121. Paris, C.; Karelovic, A.; Manrique, R.; le Bras, S.; Devred, F.; Vykoukal, V.; Styskalik, A.; Eloy, P.; Debecker, D.P. CO_2 Hydrogenation to Methanol with Ga- and Zn-Doped Mesoporous Cu/SiO2 Catalysts Prepared by the Aerosol-Assisted Sol-Gel Process. *ChemSusChem* **2020**, *13*, 6409–6417. https://doi.org/10.1002/cssc.202001951.
122. Liao, F.; Huang, Y.; Ge, J.; Zheng, W.; Tedsree, K.; Collier, P.; Hong, X.; Tsang, S.C. Morphology-Dependent Interactions of ZnO with Cu Nanoparticles at the Materials' Interface in Selective Hydrogenation of CO_2 to CH3OH. *Angew. Chem. Int. Ed.* **2011**, *50*, 2162–2165. https://doi.org/10.1002/anie.201007108.
123. San, X.; Gong, X.; Hu, Y.; Hu, Y.; Wang, G.; Qi, J.; Meng, D.; Jin, Q. Highly Dispersed Cu/Graphene Nanocatalyst Guided by MOF Structure: Application to Methanol Synthesis from CO_2 Hydrogenation. *ChemistrySelect* **2021**, *6*, 6115–6118. https://doi.org/10.1002/slct.202101179.
124. Yang, H.Y.; Gao, P.; Zhang, C.; Zhong, L.S.; Li, X.P.; Wang, S.; Wang, H.; Wei, W.; Sun, Y.H. Core-shell structured Cu@m-SiO2 and Cu/ZnO@m-SiO2 catalysts for methanol synthesis from CO_2 hydrogenation. *Catal. Commun.* **2016** *84*, 56–60. https://doi.org/10.1016/j.catcom.2016.06.010.
125. Laudenschleger, D.; Ruland, H.; Muhler, M. Identifying the nature of the active sites in methanol synthesis over Cu/ZnO/Al2O3 catalysts. *Nat. Commun.* **2020**, *11*, 1–10. https://doi.org/10.1038/s41467-020-17631-5.
126. Lunkenbein, T.; Schumann, J.; Behrens, M.; Schlög, R.; Willinger, M.G. Formation of a ZnO Overlayer in Industrial Cu/ZnO/Al_2O_3Catalysts Induced by Strong Metal-Support Interactions. *Angew. Chem. Int. Ed.* **2015**, *54*, 4544–4548. https://doi.org/10.1002/anie.201411581.
127. Jiang, F.; Yang, Y.; Wang, L.; Li, Y.F.; Fang, Z.H.; Xu, Y.B.; Liu, B.; Liu, X.H. Dependence of copper particle size and interface on methanol and CO formation in CO_2 hydrogenation over Cu@ZnO catalysts. *Catal. Sci. Technol.* **2022**, *12*, 551–564. https://doi.org/10.1039/D1CY01836A.
128. Lam, E.; Corral-Pérez, J.J.; Larmier, K.; Noh, G.; Wolf, P.; Comas-Vives, A.; Urakawa, A.; Copéret, C. CO_2 Hydrogenation on Cu/Al2O3: Role of the Metal/Support Interface in Driving Activity and Selectivity of a Bifunctional Catalyst. *Angew. Chem. Int. Ed.* **2019**, *58*, 13989–13996. https://doi.org/10.1002/anie.201908060.
129. Jensen, J.; Johannessen, T.; Wedel, S.; Livbjerg, H. A study of Cu/ZnO/Al2O3 methanol catalysts prepared by flame combustion synthesis. *J. Catal.* **2003**, *218*, 67–77. https://doi.org/10.1016/s0021-9517(03)00047-2.
130. Zhu, J.D.; Ciolca, D.N.; Liu, L.; Parastaev, A.; Kosinov, N.; Hensen, E.J.M. Flame Synthesis of Cu/ZnO-CeO2 Catalysts: Synergistic Metal-Support Interactions Promote CH3OH Selectivity in CO_2 Hydrogenation. *ACS. Catal.* **2021**, 11, 4880–4892. https://doi.org/10.1021/acscatal.1c00131.
131. van den Berg, R.; Prieto, G.; Korpershoek, G.; van der Wal, L.I.; van Bunningen, A.J.; Laegsgaard-Jorgensen, S.; de Jongh, P.E.; de Jong, K.P. Structure sensitivity of Cu and CuZn catalysts relevant to industrial methanol synthesis. *Nat. Commun.* 2016, *7*, 13057. https://doi.org/10.1038/ncomms13057.
132. Sankar, M.; He, Q.; Engel, R.V.; Sainna, M.A.; Logsdail, A.J.; Roldan, A.; Willock, D.J.; Agarwal, N.; Kiely, C.; Hutchings, G.J. Role of the Support in Gold-Containing Nanoparticles as Heterogeneous Catalysts. *Chem. Rev.* **2020**, *120*, 3890–3938. https://doi.org/10.1021/acs.chemrev.9b00662.
133. Tauster, S.J.; Fung, S.C.; Baker, R.T.K.; Horsley, J.A. Strong Interactions in Supported-Metal Catalysts. *Science* **1981**, *211*, 1121–1125. https://doi.org/10.1126/science.211.4487.1121.
134. Wang, L.; Yi, Y.H.; Guo, H.C.; Tu, X. Atmospheric Pressure and Room Temperature Synthesis of Methanol through Plas-ma-Catalytic Hydrogenation of CO_2. *Acs Catal.* **2018**, 8, 90–100.
135. Conrad, F.; Massue, C.; Kühl, S.; Kunkes, E.; Girgsdies, F.; Kasatkin, I.; Zhang, B.; Friedrich, M.; Luo, Y.; Armbrüster, M.; et al. Microwave-hydrothermal synthesis and characterization of nanostructured copper substituted ZnM2O4 (M = Al, Ga) spinels as precursors for thermally stable Cu catalysts. *Nanoscale* **2012**, *4*, 2018–2028. https://doi.org/10.1039/c2nr11804a.
136. Liang, B.; Ma, J.; Su, X.; Yang, C.; Duan, H.; Zhou, H.; Deng, S.; Li, L.; Huang, Y. Investigation on Deactivation of Cu/ZnO/Al2O3 Catalyst for CO_2 Hydrogenation to Methanol. *Ind. Eng. Chem. Res.* **2019**, *58*, 9030–9037. https://doi.org/10.1021/acs.iecr.9b01546.
137. Ye, R.-P.; Lin, L.; Li, Q.; Zhou, Z.; Wang, T.; Russell, C.K.; Adidharma, H.; Xu, Z.; Yao, Y.-G.; Fan, M. Recent progress in improving the stability of copper-based catalysts for hydrogenation of carbon–oxygen bonds. *Catal. Sci. Technol.* **2018**, *8*, 3428–3449. https://doi.org/10.1039/c8cy00608c.

138. Kurtz, M.; Wilmer, H.; Genger, T.; Hinrichsen, K.-O.; Muhler, M. Deactivation of Supported Copper Catalysts for Methanol Synthesis. *Catal. Lett.* **2003**, *86*, 77–80. https://doi.org/10.1023/a:1022663125977.
139. Hansen, P.L.; Wagner, J.B.; Helveg, S.; Rostrup-Nielsen, J.R.; Clausen, B.S.; Topsøe, H. Atom-Resolved Imaging of Dynamic Shape Changes in Supported Copper Nanocrystals. *Science* **2002**, *295*, 2053–2055. https://doi.org/10.1126/science.1069325.
140. Martinez-Suarez, L.; Frenzel, J.; Marx, D.; Meyer, B. Tuning the Reactivity of a Cu/ZnO Nanocatalyst via Gas Phase Pressure. *Phys. Rev. Lett.* **2013**, doi:10.1103/PhysRevLett.110.086108.
141. Li, C.; Yuan, X.; Fujimoto, K. Development of highly stable catalyst for methanol synthesis from carbon dioxide. *Appl. Catal. A: Gen.* **2014**, *469*, 306–311. https://doi.org/10.1016/j.apcata.2013.10.010.
142. Wilmer, H.; Hinrichsen, O. Dynamical Changes in Cu/ZnO/Al2O3 Catalysts. *Catal. Lett.* **2002**, *82*, 117–122. https://doi.org/10.1023/a:1020560628950.
143. Liu, T.K.; Xu, D.; Wu, D.D.; Liu, G.L.; Hong, X.L. Spinel ZnFe2O4 Regulates Copper Sites for CO_2 Hydrogenation to Methanol. *ACS Sustain. Chem. Eng.* **2021**, 9, 4033–4041. https://doi.org/10.1021/acssuschemeng.0c07682.
144. Li, L.; Zhang, H.B.; Zhou, P.; Meng, X.L.; Liu, L.Z.; Jia, J.P.; Sun, T.H. Three dimensional ordered macroporous zinc ferrite composited silica sorbents with promotional desulfurization and regeneration activity at mid-high temperature. *Appl. Surf. Sci.* **2019**, *470*, 177–186. https://doi.org/10.1016/j.apsusc.2018.11.033.
145. Kühl, S.; Schumann, J.; Kasatkin, I.; Hävecker, M.; Schlögl, R.; Behrens, M. Ternary and quaternary Cr or Ga-containing ex-LDH catalysts—Influence of the additional oxides onto the microstructure and activity of Cu/ZnAl2O4 catalysts. *Catal. Today* **2015**, *246*, 92–100. https://doi.org/10.1016/j.cattod.2014.08.029.
146. Wang, J.; Zeng, Z.; Li, L. Effect of Promoters on the Catalytic Performance and Properties of Cu-ZnO-Al2O3 -SiO2 Catalysts. *J. Petrochem. Univ.* **2005**, *18*, 9–14.
147. Frontera, P.; Macario, A.; Ferraro, M.; Antonucci, P. Supported Catalysts for CO_2 Methanation: A Review. *Catalysts* **2017**, *7*, 59. https://doi.org/10.3390/catal7020059.
148. Du, J.; Zhang, Y.J.; Wang, K.J.; Ding, F.; Jia, S.Y.; Liu, G.G.; Tan, L.M. Investigation on the promotional role of Ga2O3 on the CuO-ZnO/HZSM-5 catalyst for CO_2 hydrogenation. *Rsc. Adv.* **2021**, 11, 14426–14433. https://doi.org/10.1039/D0RA10849A.
149. Chen, F.; Gao, W.; Wang, K.; Wang, C.; Wu, X.; Liu, N.; Guo, X.; He, Y.; Zhang, P.; Yang, G.; et al. Enhanced performance and stability of Cu/ZnO catalyst by introducing MgO for low-temperature methanol synthesis using methanol itself as catalytic promoter. *Fuel* **2022**, *315*, 123272. https://doi.org/10.1016/j.fuel.2022.123272.
150. Lorenz, H.; Jochum, W.; Klötzer, B.; Stöger-Pollach, M.; Schwarz, S.; Pfaller, K.; Penner, S. Novel methanol steam reforming activity and selectivity of pure In2O3. *Appl. Catal. A: Gen.* **2008**, *347*, 34–42. https://doi.org/10.1016/j.apcata.2008.05.028.
151. Ye, J.; Liu, C.; Ge, Q. DFT Study of CO_2 Adsorption and Hydrogenation on the In2O3 Surface. *J. Phys. Chem. C* **2012**, *116*, 7817–7825. https://doi.org/10.1021/jp3004773.
152. Frei, M.S.; Mondelli, C.; García-Muelas, R.; Kley, K.S.; Puértolas, B.; López, N.; Safonova, O.V.; Stewart, J.A.; Ferré, D.C.; Pérez-Ramírez, J. Atomic-scale engineering of indium oxide promotion by palladium for methanol production via CO_2 hydrogenation. *Nat. Commun.* **2019**, *10*, 1–11. https://doi.org/10.1038/s41467-019-11349-9.
153. Frei, M.S.; Mondelli, C.; Garcia-Muelas, R.; Morales-Vidal, J.; Philipp, M.; Safonova, O.V.; Lopez, N.; Stewart, J.A.; Ferre, D.C.; Perez-Ramirez, J. Nanostructure of nickel-promoted indium oxide catalysts drives selectivity in CO_2 hydrogenation. *Nat. Commun.* **2021**, *12*, 1960. https://doi.org/10.1038/s41467-021-22224-x.
154. Frei, M.S.; Mondelli, C.; Perez-Ramirez, J. Development of In2O3-based Catalysts for CO_2-based Methanol Production. *Chimia* **2020**, 74, 257–262. https://doi.org/10.3929/ethz-b-000415235.
155. Jia, X.; Sun, K.; Wang, J.; Shen, C.; Liu, C.-J. Selective hydrogenation of CO_2 to methanol over Ni/In2O3 catalyst. *J. Energy Chem.* **2020**, *50*, 409–415. https://doi.org/10.1016/j.jechem.2020.03.083.
156. Rui, N.; Sun, K.H.; Shen, C.Y.; Liu, C.J. Density functional theoretical study of Au-4/In2O3 catalyst for CO_2 hydrogenation to methanol: The strong metal-support interaction and its effect. *J. CO_2 Util.* **2020**, *42*, 101313.
157. Sloczynski, J.; Grabowski, R.; Kozlowska, A.; Olszewski, P.; Stoch, J.; Skrzypek, J.; Lachowska, M. Catalytic activity of the M/(3ZnO center dot ZrO2) system (M = Cu, Ag, Au) in the hydrogenation of CO_2 to methanol. *Appl. Catal. Gen.* **2004**, *278*, 11–23. https://doi.org/10.1016/j.apcata.2004.09.014.
158. Sun, K.; Fan, Z.; Ye, J.; Yan, J.; Ge, Q.; Li, Y.; He, W.; Yang, W.; Liu, C.-J. Hydrogenation of CO_2 to methanol over In2O3 catalyst. *J. CO_2 Util.* **2015**, *12*, 1–6. https://doi.org/10.1016/j.jcou.2015.09.002.
159. Sun, K.; Rui, N.; Zhang, Z.; Sun, Z.; Ge, Q.; Liu, C.-J. A highly active Pt/In2O3 catalyst for CO_2 hydrogenation to methanol with enhanced stability. *Green Chem.* **2020**, *22*, 5059–5066. https://doi.org/10.1039/d0gc01597k.
160. Tsoukalou, A.; Abdala, P.M.; Stoian, D.; Huang, X.; Willinger, M.-G.; Fedorov, A.; Müller, C.R. Structural Evolution and Dynamics of an In2O3 Catalyst for CO_2 Hydrogenation to Methanol: An Operando XAS-XRD and In Situ TEM Study. *J. Am. Chem. Soc.* **2019**, *141*, 13497–13505. https://doi.org/10.1021/jacs.9b04873.
161. Wu, Q.; Shen, C.; Rui, N.; Sun, K.; Liu, C.-J. Experimental and theoretical studies of CO_2 hydrogenation to methanol on Ru/In2O3. *J. CO_2 Util.* **2021**, *53*, 101720. https://doi.org/10.1016/j.jcou.2021.101720.
162. Frei, M.S.; Mondelli, C.; Cesarini, A.; Krumeich, F.; Hauert, R.; Stewart, J.A.; Ferré, D.C.; Pérez-Ramírez, J. Role of Zirconia in Indium Oxide-Catalyzed CO_2 Hydrogenation to Methanol. *ACS Catal.* **2020**, *10*, 1133–1145. https://doi.org/10.1021/acscatal.9b03305.
163. Yang, C.S.; Pei, C.L.; Luo, R.; Liu, S.H.; Wang, Y.N.; Wang, Z.Y.; Zhao, Z.J.; Gong, J.L. Strong Electronic Oxide-Support Interaction over In2O3/ZrO2 for Highly Selective CO_2 Hydrogenation to Methanol. *J. Am. Chem. Soc.* **2020**, *142*, 19523–19531.

164. Grabowski, R.; Słoczyński, J.; Śliwa, M.; Mucha, D.; Socha, R.; Lachowska, M.; Skrzypek, J. Influence of Polymorphic ZrO2 Phases and the Silver Electronic State on the Activity of Ag/ZrO2 Catalysts in the Hydrogenation of CO_2 to Methanol. *ACS Catal.* **2011**, *1*, 266–278. https://doi.org/10.1021/cs100033v.
165. Baiker, A.; Kilo, M.; Maciejewski, M.; Menzi, S.; Wokaun, A.; Waugh, K.C.; Krauss, H.L.; Prins, R.; Kochloefl, K.; Holderich, W.; et al. Hydrogenation of CO_2 Over Copper, Silver And Gold Zirconia Catalysts-Comparative-Study Of Catalyst Properties and Reaction Pathways. *Stud. Surf. Sci. Catal.* **1993** *75*, 1257–1272. https://doi.org/10.1016/S0167-2991(08)64449-3.
166. Rhodes, M.D.; Bell, A.T. The effects of zirconia morphology on methanol synthesis from CO and H-2 over Cu/ZrO2 catalysts Part I. Steady-state studies. *J. Catal.* **2005**, *233*, 198–209. https://doi.org/10.1016/j.jcat.2005.04.026.
167. Ye, J.; Ge, Q.; Liu, C.J. Effect of PdIn bimetallic particle formation on CO_2 reduction over the Pd-In/SiO2 catalyst. *Chem. Eng. Sci.* **2015**, *135*, 193–201. https://doi.org/10.1016/j.ces.2015.04.034.
168. Rui, N.; Wang, Z.; Sun, K.; Ye, J.; Ge, Q.; Liu, C.-J. CO_2 hydrogenation to methanol over Pd/In2O3: effects of Pd and oxygen vacancy. *Appl. Catal. B: Environ.* **2017**, *218*, 488–497. https://doi.org/10.1016/j.apcatb.2017.06.069.
169. Han, Z.; Tang, C.Z.; Wang, J.J.; Li, L.D.; Li, C. Atomically dispersed Pt(n+) species as highly active sites in Pt/In2O3 catalysts for methanol synthesis from CO_2 hydrogenation. *J. Catal.* **2021**, *394*, 236–244. https://doi.org/10.1016/j.jcat.2020.06.018.
170. Wang, L.X.; Wang, L.; Xiao, F.S. Tuning product selectivity in CO_2 hydrogenation over metal-based catalysts. *Chem. Sci.* **2021**, *12*, 14660–14673. https://doi.org/10.1039/D1SC03109K.
171. Nerlov, J.; Chorkendorff, I. Methanol Synthesis from CO_2, CO, and H2 over Cu(100) and Ni/Cu(100). *J. Catal.* **1999**, *181*, 271–279. https://doi.org/10.1006/jcat.1998.2301.
172. Snider, J.L.; Streibel, V.; Hubert, M.A.; Choksi, T.S.; Valle, E.; Upham, D.C.; Schumann, J.; Duyar, M.S.; Gallo, A.; Abild-Pedersen, F.; et al. Revealing the Synergy between Oxide and Alloy Phases on the Performance of Bimetallic In–Pd Catalysts for CO_2 Hydrogenation to Methanol. *ACS Catal.* **2019**, *9*, 3399–3412. https://doi.org/10.1021/acscatal.8b04848.
173. Fujitani, T.; Nakamura, J.; Uchijima, T. The kinetics and mechanism of methanol synthesis by hydrogenation of CO_2 over a Zn-deposited Cu(111) surface. *Surf. Sci.* **1997**, *383*, 285–298. https://doi.org/10.1016/s0039-6028(97)00192-1.
174. Dong, Q.; Huang, Y.; Yang, H.; Pei, J.; Li, K.; Yuan, M.; Xiao, W.; Ni, W.; Hou, Z. The Catalytic Hydrogenation of Biomass Platform Molecules by Ni–Co Nanoalloy Catalysts. *Top. Catal.* **2017**, *60*, 666–676. https://doi.org/10.1007/s11244-017-0774-4.
175. Nakamura, I.; Nakano, H.; Fujitani, T.; Uchijima, T. Evidence for a special formate species adsorbed on the Cu–Zn active site for methanol synthesis. *Surf. Sci.* **1998**, *402-404*, 92–95. https://doi.org/10.1016/s0039-6028(97)00910-2.
176. Goyal, R.; Lee, W.; Sameer, S.; Sarkar, B.; Chiang, K.; Bordoloi, A. CNx stabilized Ni-Ga nanoparticles for CO_2 hydrogenation: Role of preparation methods. *Catal. Today* **2020**, *343*, 48–55. https://doi.org/10.1016/j.cattod.2019.03.031.
177. Studt, F.; Sharafutdinov, I.; Abild-Pedersen, F.; Elkjær, C.F.; Hummelshøj, J.S.; Dahl, S.; Chorkendorff, I.; Nørskov, J.K. Discovery of a Ni-Ga catalyst for carbon dioxide reduction to methanol. *Nat. Chem.* **2014**, *6*, 320–324. https://doi.org/10.1038/nchem.1873.
178. Beck, A.; Zabilskiy, M.; Newton, M.A.; Safonova, O.; Willinger, M.G.; van Bokhoven, J.A. Following the structure of cop-per-zinc-alumina across the pressure gap in carbon dioxide hydrogenation. *Nat. Catal.* **2021**, *4*, 488–497. https://doi.org/10.1038/s41929-021-00625-x.
179. Zhu, J.; Cannizzaro, F.; Liu, L.; Zhang, H.; Kosinov, N.; Filot, I.A.W.; Rabeah, J.; Brückner, A.; Hensen, E.J.M. Ni–In Synergy in CO_2 Hydrogenation to Methanol. *ACS Catal.* **2021**, *11*, 11371–11384. https://doi.org/10.1021/acscatal.1c03170.
180. An, V.; Anisimov, E.; Druzyanova, V.; Burtsev, N.; Shulepov, I.; Khaskelberg, M. Study of tribological behavior of Cu-MoS2 and Ag-MoS2 nanocomposite lubricants. *SpringerPlus* **2016**, *5*, 72. https://doi.org/10.1186/s40064-016-1702-y.
181. Tong, X.; Ashalley, E.; Lin, F.; Li, H.; Wang, Z.M. Advances in MoS2-Based Field Effect Transistors (FETs). *Nano-Micro Lett.* **2015**, *7*, 203–218. https://doi.org/10.1007/s40820-015-0034-8.
182. Xu, H.; Zhu, J.; Ma, Q.; Ma, J.; Bai, H.; Chen, L.; Mu, S. Two-Dimensional MoS_2: Structural Properties, Synthesis Methods, and Regulation Strategies toward Oxygen Reduction. *Micromachines* **2021**, *12*, 240. https://doi.org/10.3390/mi12030240.
183. Pacholik, G.; Enzlberger, L.; Benzer, A.; Rameshan, R.; Latschka, M.; Rameshan, C.; Föttinger, K. In situ XPS studies of MoS2-based CO_2 hydrogenation catalysts. *J. Phys. D: Appl. Phys.* **2021**, *54*, 324002. https://doi.org/10.1088/1361-6463/ac006f.
184. Zhang, S.-K.; Wang, H. Converting CO_2 to liquid fuel on MoS2 vacancies. *Joule* **2021**, *5*, 1038–1040. https://doi.org/10.1016/j.joule.2021.04.018.
185. Baek, D.-H.; Kim, J. MoS 2 gas sensor functionalized by Pd for the detection of hydrogen. *Sensors Actuators B: Chem.* **2017**, *250*, 686–691. https://doi.org/10.1016/j.snb.2017.05.028.
186. Song, I.; Park, C.; Choi, H.C. Synthesis and properties of molybdenum disulphide: from bulk to atomic layers. *RSC Adv.* **2015**, *5*, 7495–7514. https://doi.org/10.1039/c4ra11852a.
187. Studt, F. Catalysis by unusual vacancies. *Nat. Catal.* **2021**, *4*, 184–185. https://doi.org/10.1038/s41929-021-00593-2.
188. Centi, G. Controlled location of S vacancies in MoS2 nanosheets for high-performance hydrogenation of CO_2 to methanol. *J. Energy Chem.* **2021**, *64*, 113–115. https://doi.org/10.1016/j.jechem.2021.04.036.
189. Cui, W.-G.; Zhang, G.-Y.; Hu, T.-L.; Bu, X.-H. Metal-organic framework-based heterogeneous catalysts for the conversion of C1 chemistry: CO, CO_2 and CH_4. *Co-ord. Chem. Rev.* **2019**, *387*, 79–120. https://doi.org/10.1016/j.ccr.2019.02.001.
190. Wang, Q.; Astruc, D. State of the Art and Prospects in Metal-Organic Framework (MOF)-Based and MOF-Derived Nanocatalysis. *Chem. Rev* **2020**, *120*, 1438–1511. https://doi.org/10.1021/acs.chemrev.9b00223.

191. An, B.; Zhang, J.; Cheng, K.; Ji, P.; Wang, C.; Lin, W. Confinement of Ultrasmall Cu/ZnOx Nanoparticles in Metal–Organic Frameworks for Selective Methanol Synthesis from Catalytic Hydrogenation of CO_2. *J. Am. Chem. Soc.* **2017**, *139*, 3834–3840. https://doi.org/10.1021/jacs.7b00058.
192. Han, Y.; Xu, H.; Su, Y.; Xu, Z.-L.; Wang, K.; Wang, W. Noble metal (Pt, Au@Pd) nanoparticles supported on metal organic framework (MOF-74) nanoshuttles as high-selectivity CO_2 conversion catalysts. *J. Catal.* **2019**, *370*, 70–78. https://doi.org/10.1016/j.jcat.2018.12.005.
193. Ye, J.; Johnson, J.K. Catalytic hydrogenation of CO_2 to methanol in a Lewis pair functionalized MOF. *Catal. Sci. Technol.* **2016**, *6*, 8392–8405. https://doi.org/10.1039/c6cy01245k.
194. Gutterød, E.S.; Lazzarini, A.; Fjermestad, T.; Kaur, G.; Manzoli, M.; Bordiga, S.; Svelle, S.; Lillerud, K.P.; Skúlason, E.; Øien-Ødegaard, S.; et al. Hydrogenation of CO_2 to Methanol by Pt Nanoparticles Encapsulated in UiO-67: Deciphering the Role of the Metal–Organic Framework. *J. Am. Chem. Soc.* **2019**, *142*, 999–1009. https://doi.org/10.1021/jacs.9b10873.
195. Li, L.S.; Pan, X.B.; Lan, D.P.; Xu, H.T.; Ge, J.P.; Zhang, H.Q.; Zheng, Z.Z.; Liu, J.C.; Xu, Z.L.; Liu, J.K. Etching of cubic Pd@Pt in UiO-66 to obtain nanocages for enhancing CO_2 hydrogenation. *Mater. Today Energy* **2021**, 19, 7. https://doi.org/10.1016/j.mtener.2020.100585.
196. Wang, J.J.; Li, G.N.; Li, Z.L.; Tang, C.Z.; Feng, Z.C.; An, H.Y.; Liu, H.L.; Liu, T.F.; Li, C. A highly selective and stable ZnO-ZrO2 solid solution catalyst for CO_2 hydrogenation to methanol. *Sci. Adv.* **2017**, *3*. https://doi.org/10.1126/sciadv.1701290.
197. Wang, J.J.; Tang, C.Z.; Li, G.N.; Han, Z.; Li, Z.L.; Liu, H.; Cheng, F.; Li, C. High-Performance MaZrOx (M-a = Cd, Ga) Solid-Solution Catalysts for CO_2 Hydrogenation to Methanol. *ACS Catal.* **2019**, *9*, 10253–10259. https://doi.org/10.1021/acscatal.9b03449.
198. Huang, C.; Wu, Z.; Luo, H.; Zhang, S.; Shao, Z.; Wang, H.; Sun, Y. CO_2 Hydrogenation to Methanol over PdZnZr Solid Solution: Effects of the PdZn Alloy and Oxygen Vacancy. *ACS Appl. Energy Mater.* **2021**, *4*, 9258–9266. https://doi.org/10.1021/acsaem.1c01502.
199. Schlogl, R. Heterogeneous Catalysis. Angew. *Chem.Int. Edit* **2015**, *54*, 3465–3520. https://doi.org/10.1002/anie.201410738.
200. Pan, Y.; Shen, X.; Yao, L.; Bentalib, A.; Peng, Z. Active Sites in Heterogeneous Catalytic Reaction on Metal and Metal Oxide: Theory and Practice. *Catalysts* **2018**, *8*, 478. https://doi.org/10.3390/catal8100478.
201. Qiu, H. Exploring the reaction mechanism of heterogeneous catalysis with surface science. In *Catalysis: Volume 32*; Spivey, J., Han, Y., Shekhawat, D., Eds.; Royal Society of Chemistry: London, UK, 2020; pp. 188–202. https://doi.org/10.1039/9781788019477-00188.
202. Freund, H.-J. Models for heterogeneous catalysts: studies at the atomic level. *Rend. Lince* **2016**, *28*, 5–18. https://doi.org/10.1007/s12210-016-0560-4.
203. McClure, S.M.; Goodman, D.W. New insights into catalytic CO oxidation on Pt-group metals at elevated pressures. *Chem. Phys. Lett.* **2009**, *469*, 1–13. https://doi.org/10.1016/j.cplett.2008.12.066.
204. Ertl, G. Reactions at Surfaces: From Atoms to Complexity (Nobel Lecture). *Angew. Chem. Int. Ed.* **2008**, *47*, 3524–3535. https://doi.org/10.1002/anie.200800480.
205. Szanyi, J.; Goodman, D.W. Methanol synthesis on a Cu(100) catalyst. *Catal. Lett.* **1991**, 10, 383–390. https://doi.org/10.1007/BF00769173.
206. Rasmussen, P.; Kazuta, M.; Chorkendorff, I. Synthesis of methanol from a mixture of H2 and CO_2 on Cu(100). *Surf. Sci.* **1994**, *318*, 267–280. https://doi.org/10.1016/0039-6028(94)90101-5.
207. Nerlov, J.; Chorkendorff, I. Promotion through gas phase induced surface segregation: methanol synthesis from CO, CO_2 and H2 over Ni/Cu(100). *Catal. Lett.* **1998**, *54*, 171–176. https://doi.org/10.1023/a:1019033517855.
208. Liu, Y.-M.; Liu, J.-T.; Liu, S.; Li, J.; Gao, Z.-H.; Zuo, Z.-J.; Huang, W. Reaction mechanisms of methanol synthesis from CO/CO_2 hydrogenation on Cu 2 O(111): Comparison with Cu(111). *J. CO_2 Util.* **2017**, *20*, 59–65. https://doi.org/10.1016/j.jcou.2017.05.005.
209. Yoshihara, J; Parker, S.; Schafer, A.; Campbell, C.T. Methanol synthesis and reverse water-gas shift kinetics over clean poly-crystalline copper. *Catal. Lett.* **1995**, 31, 313–324. https://doi.org/10.1007/BF00808595.
210. Yoshihara, J.; Campbell, C.T. Methanol Synthesis and Reverse Water–Gas Shift Kinetics over Cu(110) Model Catalysts: Structural Sensitivity. *J. Catal.* **1996**, *161*, 776–782. https://doi.org/10.1006/jcat.1996.0240.
211. Kim, Y.; Trung, T.S.B.; Yang, S.; Kim, S.; Lee, H. Mechanism of the Surface Hydrogen Induced Conversion of CO_2 to Methanol at Cu(111) Step Sites. *ACS Catal.* **2016**, *6*, 1037–1044. https://doi.org/10.1021/acscatal.5b02083.
212. van Spronsen, M.A.; Frenken, J.W.M.; Groot, I.M.N. Surface science under reaction conditions: CO oxidation on Pt and Pd model catalysts. *Chem. Soc. Rev.* **2017**, *46*, 4347–4374. https://doi.org/10.1039/c7cs00045f.
213. Feng, K.; Wang, Y.; Guo, M.; Zhang, J.; Li, Z.; Deng, T.; Zhang, Z.; Yan, B. In-situ/operando techniques to identify active sites for thermochemical conversion of CO_2 over heterogeneous catalysts. *J. Energy Chem.* **2021**, *62*, 153–171. https://doi.org/10.1016/j.jechem.2021.03.054.
214. Ren, Y.; Yuan, K.; Zhou, X.; Sun, H.; Wu, K.; Bernasek, S.L.; Chen, W.; Xu, G.Q. Catalytic Intermediates of CO_2 Hydrogenation on Cu(111) Probed by In Operando Near-Ambient Pressure Technique. *Chem. A. Eur. J.* **2018**, *24*, 16097–16103. https://doi.org/10.1002/chem.201802931.
215. Tauster, S.J.; Fung, S.C.; Garten, R.L. Strong metal-support interactions. Group 8 noble metals supported on titanium dioxide. *J. Am. Chem. Soc.* **1978**, *100*, 170–175. https://doi.org/10.1021/ja00469a029.
216. Tauster, S.J. Strong Metal-Support Interactions. *Acc. Chem. Res.* **1987**, 20, 389–394. https://doi.org/10.1021/ar00143a001.

217. Tauster, S.J.; Fung, S.C. Strong Metal-Support Interactions: Occurrence among the Binary Oxides of Group IIA-VB. *J. Catal.* ***1978***, 55, 29–35. https://doi.org/10.1016/0021-9517(78)90182-3.
218. Liu, X.; Liu, M.-H.; Luo, Y.-C.; Mou, C.-Y.; Lin, S.D.; Cheng, H.; Chen, J.-M.; Lee, J.-F.; Lin, T.-S. Strong Metal–Support Interactions between Gold Nanoparticles and ZnO Nanorods in CO Oxidation. *J. Am. Chem. Soc.* **2012**, *134*, 10251–10258. https://doi.org/10.1021/ja3033235.
219. Qiu, H.; Gallino, F.; Di Valentin, C.; Wang, Y. Shallow Donor States Induced by In-Diffused Cu in ZnO: A Combined HREELS and Hybrid DFT Study. *Phys. Rev. Lett.* **2011**, *106*. https://doi.org/10.1103/physrevlett.106.066401.
220. Fujitani, T.; Nakamura, I.; Watanabe, T.; Uchijima, T.; Nakamura, J. Methanol synthesis by the hydrogenation of CO_2 over Zn-deposited Cu(111) and Cu(110) surfaces. *Catal. Lett.* **1995**, *35*, 297–302. https://doi.org/10.1007/bf00807186.
221. Nakamura, J.; Uchijima, T.; Kanai, Y.; Watanabe, T.; Saito, M.; Fujitani, T. A Surface Science Investigation of Methanol Synthesis over a Zn-Deposited Polycrystalline Cu Surface. *J. Catal.* **1996**, *160*, 65–75. https://doi.org/10.1006/jcat.1996.0124.
222. Kanai, Y.; Watanabe, T.; Fujitani, T.; Uchijima, T.; Nakamura, J. The synergy between Cu and ZnO in methanol synthesis catalysts. *Catal. Lett.* **1996**, *38*, 157–163. https://doi.org/10.1007/bf00806562.
223. Batyrev, E.D.; Shiju, N.R.; Rothenberg, G. Exploring the Activated State of Cu/ZnO(0001)–Zn, a Model Catalyst for Methanol Synthesis. *J. Phys. Chem. C* **2012**, *116*, 19335–19341. https://doi.org/10.1021/jp3051438.
224. Palomino, R.M.; Ramírez, P.J.; Liu, Z.; Hamlyn, R.; Waluyo, I.; Mahapatra, M.; Orozco, I.; Hunt, A.; Simonovis, J.P.; Senanayake, S.D.; et al. Hydrogenation of CO_2 on ZnO/Cu(100) and ZnO/Cu(111) Catalysts: Role of Copper Structure and Metal–Oxide Interface in Methanol Synthesis. *J. Phys. Chem. B* **2017**, *122*, 794–800. https://doi.org/10.1021/acs.jpcb.7b06901.
225. Fujitani, T.; Nakamura, J. The effect of ZnO in methanol synthesis catalysts on Cu dispersion and the specific activity. *Catal. Lett.* **1998**, *56*, 119–124. https://doi.org/10.1023/a:1019000927366.
226. Schott, V.; Oberhofer, H.; Birkner, A.; Xu, M.; Wang, Y.; Muhler, M.; Reuter, K.; Wöll, C. Corrigendum: Chemical Activity of Thin Oxide Layers: Strong Interactions with the Support Yield a New Thin-Film Phase of ZnO. *Angew. Chem. Int. Ed.* **2017**, *56*, 12399. https://doi.org/10.1002/anie.201708864.
227. Schott, V.; Oberhofer, H.; Birkner, A.; Xu, M.; Wang, Y.; Muhler, M.; Reuter, K.; Wöll, C. Chemical Activity of Thin Oxide Layers: Strong Interactions with the Support Yield a New Thin-Film Phase of ZnO. *Angew. Chem. Int. Ed.* **2013**, *52*, 11925–11929. https://doi.org/10.1002/anie.201302315.
228. Lunkenbein, T.; Girgsdies, F.; Kandemir, T.; Thomas, L.; Behrens, M.; Schlögl, R.; Frei, E. Bridging the Time Gap: A Copper/Zinc Oxide/Aluminum Oxide Catalyst for Methanol Synthesis Studied under Industrially Relevant Conditions and Time Scales. *Angew. Chem. Int. Ed.* **2016**, *55*, 12708–12712. https://doi.org/10.1002/anie.201603368.
229. Fichtl, M.B.; Schlereth, D.; Jacobsen, N.; Kasatkin, I.; Schumann, J.; Behrens, M.; Schlögl, R.; Hinrichsen, O. Kinetics of deactivation on Cu/ZnO/Al2O3 methanol synthesis catalysts. *Appl. Catal. A: Gen.* **2015**, *502*, 262–270. https://doi.org/10.1016/j.apcata.2015.06.014.
230. Nakamura, J.; Choi, Y.; Fujitani, T. On the Issue of the Active Site and the Role of ZnO in Cu/ZnO Methanol Synthesis Catalysts. *Top. Catal.* **2003**, *22*, 277–285. https://doi.org/10.1023/a:1023588322846.
231. Wu, X.-K.; Yan, H.-M.; Zhang, W.; Zhang, J.; Xia, G.-J.; Wang, Y.-G. Unraveling the catalytically active phase of carbon dioxide hydrogenation to methanol on Zn/Cu alloy: Single atom versus small cluster. *J. Energy Chem.* **2021**, *61*, 582–593. https://doi.org/10.1016/j.jechem.2021.02.016.
232. Wu, P.P.; Yang, B. Significance of Surface Formate Coverage on the Reaction Kinetics of Methanol Synthesis from CO_2 Hydrogenation over Cu. *ACS Catal.* **2017**, *7*, 7187–7195. https://doi.org/10.1021/acscatal.7b01910.
233. Graciani, J.; Mudiyanselage, K.; Xu, F.; Baber, A.E.; Evans, J.; Senanayake, S.D.; Stacchiola, D.J.; Liu, P.; Hrbek, J.; Fernández Sanz, J.; et al. Highly active copper-ceria and copper-ceria-titania catalysts for methanol synthesis from CO_2. *Science* **2014**, *345*, 546–550. https://doi.org/10.1126/science.1253057.
234. Yang, Y.; Evans, J.; Rodriguez, J.A.; White, M.G.; Liu, P. Fundamental studies of methanol synthesis from CO_2 hydrogenation on Cu(111), Cu clusters, and Cu/ZnO(0001). *Phys. Chem. Chem. Phys.* **2010**, *12*, 9909–9917. https://doi.org/10.1039/c001484b.
235. Zhou, X.; Qu, J.; Xu, F.; Hu, J.; Foord, J.S.; Zeng, Z.; Hong, X.; Tsang, S.C.E. Shape selective plate-form Ga2O3 with strong metal-support interaction to overlying Pd for hydrogenation of CO_2 to CH3OH. *Chem. Commun.* **2013**, *49*, 1747–1749. https://doi.org/10.1039/C3CC38455A.
236. Yang, X.; Kattel, S.; Senanayake, S.D.; Boscoboinik, J.A.; Nie, X.; Graciani, J.; Rodriguez, J.A.; Liu, P.; Stacchiola, D.J.; Chen, J.G. Low Pressure CO_2 Hydrogenation to Methanol over Gold Nanoparticles Activated on a CeOx/TiO2 Interface. *J. Am. Chem. Soc.* **2015**, *137*, 10104–10107. https://doi.org/10.1021/jacs.5b06150.
237. Larmier, K.; Liao, W.-C.; Tada, S.; Lam, E.; Verel, R.; Bansode, A.; Urakawa, A.; Comas-Vives, A.; Copéret, C. CO_2 -to-Methanol Hydrogenation on Zirconia-Supported Copper Nanoparticles: Reaction Intermediates and the Role of the Metal-Support Interface. *Angew. Chem. Int. Ed.* **2017**, *56*, 2318–2323. https://doi.org/10.1002/anie.201610166.
238. Haruta, M. Size- and support-dependency in the catalysis of gold. *Catal. Today* **1997**, *36*, 153–166. https://doi.org/10.1016/s0920-5861(96)00208-8.
239. Valden, M.; Lai, X.; Goodman, D.W. Onset of Catalytic Activity of Gold Clusters on Titania with the Appearance of Nonmetallic Properties. *Science* **1998**, *281*, 1647–1650. https://doi.org/10.1126/science.281.5383.1647.
240. Nørskov, J.K.; Bligaard, T.; Hvolbæk, B.; Abild-Pedersen, F.; Chorkendorff, I.; Christensen, C.H. The nature of the active site in heterogeneous metal catalysis. *Chem. Soc. Rev.* **2008**, *37*, 2163–2171. https://doi.org/10.1039/b800260f.

241. Bredow, T.; Giordano, L.; Cinquini, F.; Pacchioni, G. Electronic properties of rutile TiO2 ultrathin films: Odd-even oscillations with the number of layers. *Phys. Rev. B*. **2004**, *70*. https://doi.org/10.1103/PhysRevB.70.035419.
242. Che, M.; Bennett, C.O. The Influence of Particle Size on the Catalytic Properties of Supported Metals. *Adv. Catal.* **1989**, *36*, 55–172. https://doi.org/10.1016/s0360-0564(08)60017-6.
243. Claus, P.; Bruckner, A.; Mohr, C.; Hofmeister, H. Supported gold nanoparticles from quantum dot to mesoscopic size scale: Effect of electronic and structural properties on catalytic hydrogenation of conjugated functional *groups. J. Am. Chem. Soc*. **2000**, *122*, 11430–1143. https://doi.org/10.1021/ja0012974.
244. Yang, B.; Liu, C.; Halder, A.; Tyo, E.C.; Martinson, A.B.F.; Seifert, S.; Zapol, P.; Curtiss, L.A.; Vajda, S. Copper Cluster Size Effect in Methanol Synthesis from CO_2. *J. Phys. Chem. C* **2017**, *121*, 10406–10412. https://doi.org/10.1021/acs.jpcc.7b01835.
245. Zhang, X.; Liu, J.-X.; Zijlstra, B.; Filot, I.A.; Zhou, Z.; Sun, S.; Hensen, E.J. Optimum Cu nanoparticle catalysts for CO_2 hydrogenation towards methanol. *Nano Energy* **2018**, *43*, 200–209. https://doi.org/10.1016/j.nanoen.2017.11.021.
246. Karelovic, A.; Ruiz, P. The role of copper particle size in low pressure methanol synthesis via CO_2 hydrogenation over Cu/ZnO catalysts. *Catal. Sci. Technol.* **2015**, *5*, 869–881. https://doi.org/10.1039/c4cy00848k.
247. Jacquemin, M.; Beuls, A.; Ruiz, P. Catalytic production of methane from CO_2 and H2 at low temperature: Insight on the reaction mechanism. *Catal. Today* **2010**, *157*, 462–466. https://doi.org/10.1016/j.cattod.2010.06.016.
248. Hulea, V.; Brunel, D.; Galarneau, A.; Philippot, K.; Chaudret, B.; Kooyman, P.; Fajula, F. Synthesis of well-dispersed ruthenium nanoparticles inside mesostructured porous silica under mild conditions. *Microporous Mesoporous Mater.* **2005**, *79*, 185–194. https://doi.org/10.1016/j.micromeso.2004.10.041.
249. Cuenya, B.R.; Behafarid, F. Nanocatalysis: size- and shape-dependent chemisorption and catalytic reactivity. *Surf. Sci. Rep.* **2015**, *70*, 135–187. https://doi.org/10.1016/j.surfrep.2015.01.001.
250. Campbell, C.T. Electronic perturbations. *Nat. Chem.* **2012**, *4*, 597–598. https://doi.org/10.1038/nchem.1412.
251. Abdel-Mageed, A.M.; Klyushin, A.Y.; Knop-Gericke, A.; Schlögl, R.; Behm, R.J. Influence of CO on the Activation, O-Vacancy Formation, and Performance of Au/ZnO Catalysts in CO_2 Hydrogenation to Methanol. *J. Phys. Chem. Lett.* **2019**, *10*, 3645–3653. https://doi.org/10.1021/acs.jpclett.9b00925.
252. Guo, X.; Zhou, R. A new insight into the morphology effect of ceria on CuO/CeO_2 catalysts for CO selective oxidation in hydrogen-rich gas. *Catal. Sci. Technol.* **2016**, *6*, 3862–3871.
253. Samson, K.; Śliwa, M.; Socha, R.P.; Góra-Marek, K.; Mucha, D.; Rutkowska-Zbik, D.; Paul, J.-F.; Ruggiero-Mikołajczyk, M.; Grabowski, R.; Słoczyński, J. Influence of ZrO2 Structure and Copper Electronic State on Activity of Cu/ZrO2 Catalysts in Methanol Synthesis from CO_2. *ACS Catal.* **2014**, *4*, 3730–3741. https://doi.org/10.1021/cs500979c.
254. Yang, Z.; He, B.; Lu, Z.; Hermansson, K. Physisorbed, chemisorbed, and oxidized CO on highly active Cu-CeO2(111). *J. Phys. Chem. C*. **2010**, *114*, 4486–4494. https://doi.org/10.1021/jp909174u.
255. Volnina, E.A.; Kipnis, M.A. Modern View of the Mechanism of Methanol Synthesis on Cu-Containing Catalysts. *Kinet. Catal.* **2020**, *61*, 119–129. https://doi.org/10.1134/s0023158420010115.
256. Schumacher, N.; Andersson, K.; Nerlov, J.; Chorkendorff, I. Formate stability and carbonate hydrogenation on strained Cu overlayers on Pt(111). *Surf. Sci.* **2008**, *602*, 2783–2788. https://doi.org/10.1016/j.susc.2008.07.003.
257. Shen, C.Y.; Bao, Q.Q.; Xue, W.J.; Sun, K.H.; Zhang, Z.T.; Jia, X.Y.; Mei, D.H.; Liu, C.J. Synergistic effect of the metal-support interaction and interfacial oxygen vacancy for CO_2 hydrogenation to methanol over Ni/In2O3 catalyst: A theoretical study. *J. Energy Chem.* **2022**, 65, 623–629.
258. Bañares, M.A. Operando methodology: combination of in situ spectroscopy and simultaneous activity measurements under catalytic reaction conditions. *Catal. Today* **2005**, *100*, 71–77. https://doi.org/10.1016/j.cattod.2004.12.017.
259. Gurlo, A.; Riedel, R. In Situ and Operando Spectroscopy for Assessing Mechanisms of Gas Sensing. *Angew. Chem. Int. Ed.* **2007**, *46*, 3826–3848. https://doi.org/10.1002/anie.200602597.
260. Weckhuysen, B.M. Snapshots of a working catalyst: possibilities and limitations of in situ spectroscopy in the field of heterogeneous catalysis, *Chem. Commun.* **2002**, doi:10.1039/B107686H.
261. Weckhuysen, B.M. Operando spectroscopy: fundamental and technical aspects of spectroscopy of catalysts under working conditions. *Phys. Chem. Chem. Phys.* **2003**, *5*, 4351–4360. https://doi.org/10.1039/b309654h.
262. Zhang, Y.; Fu, D.; Liu, X.; Zhang, Z.; Zhang, C.; Shi, B.; Xu, J.; Han, Y.-F. Operando Spectroscopic Study of Dynamic Structure of Iron Oxide Catalysts during CO_2 Hydrogenation. *ChemCatChem* **2018**, *10*, 1272–1276. https://doi.org/10.1002/cctc.201701779.
263. Chen, Z.; Wang, H.; Su, N.Q.; Duan, S.; Shen, T.; Xu, X. Beyond Mean-Field Microkinetics: Toward Accurate and Efficient Theoretical Modeling in Heterogeneous Catalysis. *ACS Catal.* **2018**, *8*, 5816–5826. https://doi.org/10.1021/acscatal.8b00943.
264. Liu, L.; Yu, M.; Hou, B.; Wang, Q.; Zhu, B.; Jia, L.; Li, D. Morphology evolution of fcc Ru nanoparticles under hydrogen atmosphere. *Nanoscale* **2019**, *11*, 8037–8046. https://doi.org/10.1039/c9nr01611b.
265. Van Rensburg, W.J.; Petersen, M.A.; Datt, M.S.; Berg, J.-A.V.D.; Van Helden, P. On the Kinetic Interpretation of DFT-Derived Energy Profiles: Cu-Catalyzed Methanol Synthesis. *Catal. Lett.* **2014**, *145*, 559–568. https://doi.org/10.1007/s10562-014-1407-1.
266. Chen, A.; Zhang, X.; Zhou, Z. Machine learning: Accelerating materials development for energy storage and conversion. *InfoMat* **2020**, *2*, 553–576. https://doi.org/10.1002/inf2.12094.

267. Lamoureux, P.S.; Winther, K.T.; Torres, J.A.G.; Streibel, V.; Zhao, M.; Bajdich, M.; Abild-Pedersen, F.; Bligaard, T. Machine Learning for Computational Heterogeneous Catalysis. *ChemCatChem* **2019**, *11*, 3581–3601. https://doi.org/10.1002/cctc.201900595.
268. Roy, D.; Mandal, S.C.; Pathak, B. Machine Learning-Driven High-Throughput Screening of Alloy-Based Catalysts for Selective CO_2 Hydrogenation to Methanol. *ACS Appl. Mater. Interfaces* **2021**, *13*, 56151–56163. https://doi.org/10.1021/acsami.1c16696.